Article

Sacrificial capillary pumps to engineer multiscalar biological forms

https://doi.org/10.1038/s41586-024-08175-5

Received: 16 October 2023

Accepted: 8 October 2024

Published online: 11 December 2024

Check for updates

Subramanian Sundaram[1,2,3]✉, Joshua H. Lee[1,2], Isabel M. Bjørge[1,2,4], Christos Michas[1,2,5], Sudong Kim[1,2,3], Alex Lammers[1,2,3], João F. Mano[4], Jeroen Eyckmans[1,2,3], Alice E. White[5,6,7] & Christopher S. Chen[1,2,3]✉

Natural tissues are composed of diverse cells and extracellular materials whose arrangements across several length scales—from subcellular lengths[1] (micrometre) to the organ scale[2] (centimetre)—regulate biological functions. Tissue-fabrication methods have progressed to large constructs, for example, through stereolithography[3] and nozzle-based bioprinting[4,5], and subcellular resolution through subtractive photoablation[6–8]. However, additive bioprinting struggles with sub-nozzle/voxel features[9] and photoablation is restricted to small volumes by prohibitive heat generation and time[10]. Building across several length scales with temperature-sensitive, water-based soft biological matter has emerged as a critical challenge, leaving large classes of biological motifs—such as multiscalar vascular trees with varying calibres—inaccessible with present technologies[11,12]. Here we use gallium-based engineered sacrificial capillary pumps for evacuation (ESCAPE) during moulding to generate multiscalar structures in soft natural hydrogels, achieving both cellular-scale (<10 μm) and millimetre-scale features. Decoupling the biomaterial of interest from the process of constructing the geometry allows non-biocompatible tools to create the initial geometry. As an exemplar, we fabricated branched, cell-laden vascular trees in collagen, spanning approximately 300-μm arterioles down to the microvasculature (roughly ten times smaller). The same approach can micropattern the inner surface of vascular walls with topographical cues to orient cells in 3D and engineer fine structures such as vascular malformations. ESCAPE moulding enables the fabrication of multiscalar forms in soft biomaterials, paving the way for a wide range of tissue architectures that were previously inaccessible in vitro.

An ever-expanding toolkit of printing technologies can build complex 3D shapes[13] ranging from the nanoscale[14] to architectural scales[15]. Yet only a very small subset of these processes function in environments suitable for cells and natural extracellular matrices (ECMs) or yield scaffolds fit for cell culture. Emerging technologies such as two-photon lithography can print complex 3D shapes with hydrogels[16], but not with natural ECMs and are limited to tailored materials, small print volumes and ultralow throughput. To tackle the present bottleneck in engineering multiscalar biological structures, we sought to develop moulding approaches for a range of natural ECMs (such as collagen and fibrin). Moulding can copy 3D shapes into soft natural ECMs starting from complex moulds, independent of how those moulds were originally formed[17], unlike bioprinting approaches that build shapes from scratch. As such, successful templating strategies would expand the range of 3D-printing processes (including non-biocompatible processes) used for the fabrication of biological structures. Sacrificial-template-based moulding of soft ECMs has been extensively explored with both soft[18,19] and rigid templates[20], but no single approach can mould both cellular-scale (<10 μm) and millimetre-scale 3D features. Sacrificial gel printing[18] does not produce micrometre-scale resolution, sharp corners or abruptly changing geometries owing to nozzle-based deposition and the fragility, surface tension and slow kinetics inherent to the printing inks. Photolithographic templating methods[21] that achieve a broad range of in-plane dimensions can mould 2.5D geometries (without overhangs) but not free-form 3D structures. Fundamentally, the challenge stems from the competing mechanical requirements: rigid templates that mould small features with high geometric fidelity are difficult to remove without destroying the surrounding soft biological material (especially for free-form 3D moulds), whereas soft templates such as sacrificial gels that are easily removed do not replicate sharp microscale features faithfully.

Ga as a sacrificial template

We reasoned that gallium is an ideal templating material to copy multiscalar biological structures into natural ECMs because: (1) its melting

[1]Biological Design Center, Boston University, Boston, MA, USA. [2]Department of Biomedical Engineering, Boston University, Boston, MA, USA. [3]Wyss Institute for Biologically Inspired Engineering, Harvard University, Boston, MA, USA. [4]Department of Chemistry, CICECO - Aveiro Institute of Materials, University of Aveiro, Campus Universitário de Santiago, Aveiro, Portugal. [5]Department of Mechanical Engineering, Boston University, Boston, MA, USA. [6]Department of Physics, Boston University, Boston, MA, USA. [7]Department of Material Science and Engineering, Boston University, Boston, MA, USA. ✉e-mail: subras@bu.edu; chencs@bu.edu

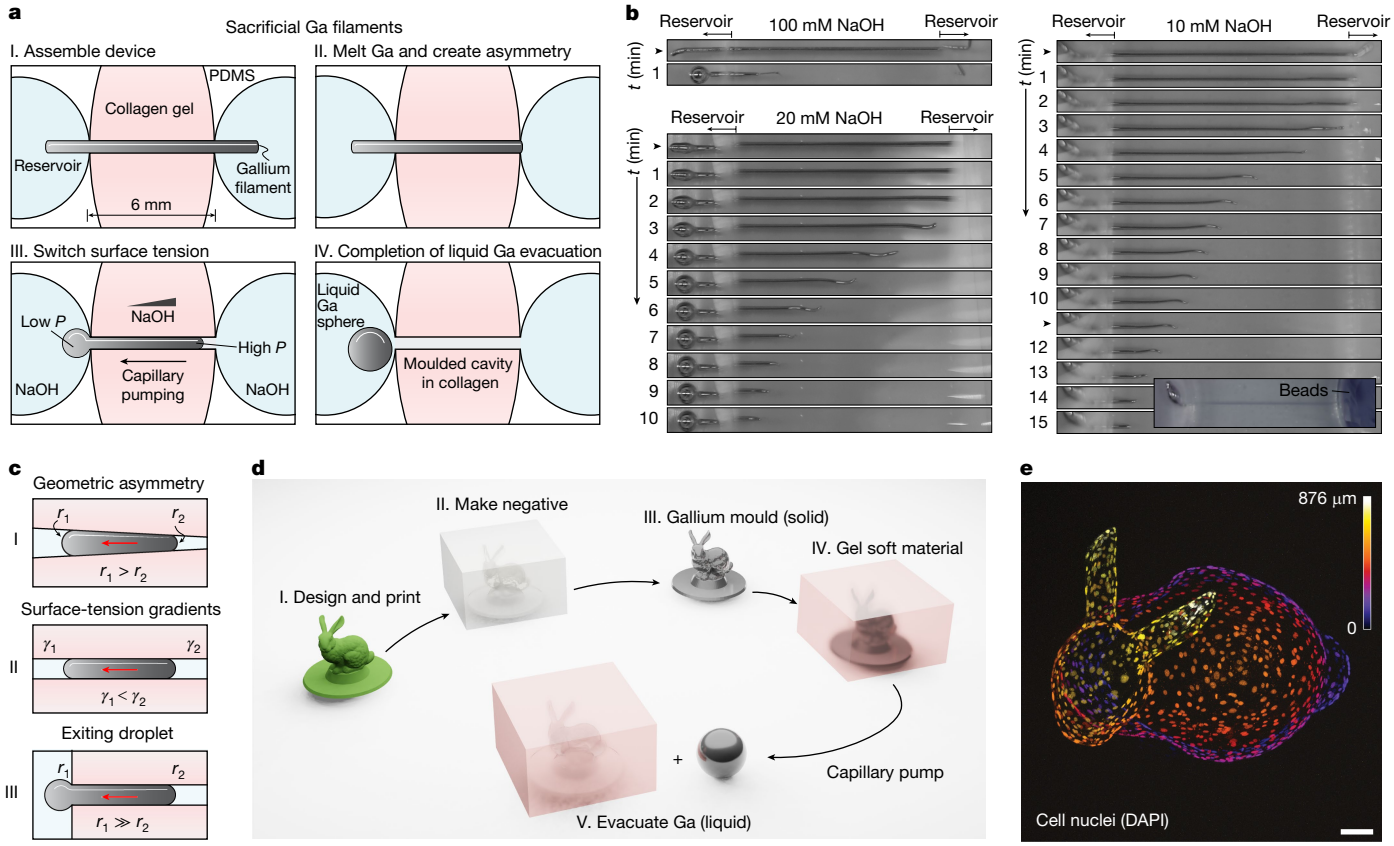

Fig. 1 | Capillary pumps for sacrificial moulding. a, Gallium filaments (150 μm diameter) are assembled into a PDMS device and collagen is polymerized in the central gel region. Subsequently, gallium is melted and one exposed filament section is severed (right reservoir in schematic), creating a geometric asymmetry. Removing the native oxide raises the surface tension, causing the liquid plug to evacuate to the side with lower Laplace pressure. **b**, When 100 mM NaOH is used for evacuation, the entire length is evacuated rapidly (roughly 1 min) but often breaks the liquid plug into several pieces. Controlled, gradual evacuation is observed with 20 mM and 10 mM NaOH (see Supplementary Videos 2–5); arrows indicate when NaOH solution was added. Inset shows the cylindrical cavity visualized with coloured beads. **c**, The Laplacian pressure across an interface is determined by the surface tension (γ) and the principal curvatures (r^{-1}). When a high-surface-tension droplet is physically constrained, the resulting differences in capillary forces cause directional flows. In the presence of geometric asymmetries (I), for example, narrowing towards one direction, capillary pumps drive liquids against this narrowing. Surface-tension gradients (II) cause similar movement in the absence of any geometric variations. A liquid droplet exiting an opening (III) experiences lower curvature at the exit, forcing complete evacuation. **d**, ESCAPE steps are as follows: the intended design is fabricated using any process (I) and a Ga cast is made through replica moulding (II and III). Soft ECMs are polymerized around the solid Ga cast (IV). Finally, capillary pumps are used to extract Ga (liquid) without disturbing the soft material (V). **e**, On Ga removal, cells are seeded into the Stanford-bunny-shaped cavity. The image shows a depth-coded projection of cell nuclei labelled with DAPI. Scale bar, 100 μm.

point (about 29.8 °C) is near cell-culture temperatures, enabling its use as both an injectable liquid[22–24] and a resilient solid casting material[25], as well as a low-viscosity liquid[22] for demoulding in the presence of natural ECMs and (2) its tunable surface oxide[26] enables the use of capillary forces in the demoulding process, conferring both spatial control and the ability to evacuate complex features hierarchically (as Laplacian pressure is inversely proportional to the feature size). The surface oxide of gallium is amphoteric and is removed by both acids and bases; however, the high concentrations typically used (about 1 M HCl or 1 M NaOH)[27] degrade natural ECMs rapidly. From the Pourbaix chart of the gallium–water system[28], we posited that milder bases will gradually remove the surface oxide without affecting natural ECMs and would drive controlled capillary pumping of liquid gallium in water-based environments, including hydrogels. Furthermore, Ga is dislodged easily from hydrogel surfaces, in contrast to polydimethylsiloxane (PDMS) surfaces (see Methods), making oxide removal with milder bases practical (Supplementary Fig. 1 and Supplementary Video 1).

We then assembled gallium filaments (150 μm diameter) to span 6-mm-wide chambers and polymerized collagen around the filaments (Fig. 1a). On melting Ga (see Methods) and removing its surface oxide with NaOH (high interfacial tension state), the geometric asymmetry between the two filament ends causes a Laplacian pressure difference that drives unidirectional capillary flow. At NaOH concentrations of 100 mM (Fig. 1b and Supplementary Video 2) or 50 mM (Supplementary Video 3), liquid Ga rapidly extracts itself from the gel (typically <1 min). Abrupt surface-tension changes lead to inconsistent evacuation, at times fragmenting the liquid plug into several pieces. With 20 mM and 10 mM NaOH, however, gradual surface oxide removal allowed liquid gallium to consistently evacuate as one non-fragmented plug (Supplementary Videos 4 and 5); the resulting conduit in the collagen gel is visualized with coloured beads (Fig. 1b, inset). To assess the dimensional stability of collagen, we performed second-harmonic generation (SHG) imaging of preformed collagen cavities exposed to NaOH. Sharp boundaries and dimensional accuracy were preserved after 30 min exposure to NaOH concentrations of 20 mM NaOH or lower (Extended Data Fig. 1a–c), but substantial dimensional changes and edge blurring were observed at 50 mM. At 100 mM NaOH, the gel boundaries could not be identified clearly. Furthermore, SHG imaging revealed that the fibrillar architecture of bulk collagen was not substantially altered at NaOH concentrations up to 20 mM (30 min exposure) but was affected at 50 mM and higher (Extended Data Fig. 1d,e). Therefore, we typically use 10 mM or 20 mM NaOH in further experiments.

Theoretical considerations

We next consider the theoretical factors for efficient unidirectional capillary pumping of liquid gallium (Fig. 1c). Pure gallium (without its native oxide) exhibits an approximately 180° contact angle in water-based environments owing to its high surface tension[29] (about 708 mN m^{-1}). The local Laplace pressure at the gallium–water interface is $2\gamma/r$, in which γ is the interfacial tension and r is the principal radius of curvature. Laplace pressure differentials result from geometric asymmetries[30] (case I in Fig. 1c), surface-tension gradients (case II) or from a droplet exiting a constricted region (case III; a special case of I). In cases I and II, liquid plugs undergo unidirectional flow when constrained by rigid walls that counter the forces exerted by gallium. When surrounded by soft gels, the internal pressure of gallium can dominate, allowing it to form a spherical droplet, deforming the gel (termed elastocapillarity[31,32]) and entrapping itself (Supplementary Fig. 2a). To be effectively rigid and prevent Ga entrapment, the elastic modulus of the surrounding material must exceed $3\gamma/r$ (Supplementary Fig. 2b; full derivation in Supplementary Information); natural ECMs are softer than this threshold for values of r below the capillary length of gallium (Supplementary Fig. 2c). Thus, in contrast to surrounding matrices such as PDMS (modulus on the order of MPa), to evacuate gallium reliably from within soft ECMs (moduli approximately 100 Pa), the lowest Laplacian pressure is maintained outside the structure being evacuated (as in case III of Fig. 1c). In practice, this is achieved with a bulb of gallium at the collecting end of the mould.

Exemplar topologies

The ESCAPE moulding process for forming 3D structures in ECMs is illustrated in Fig. 1d using the Stanford bunny design (see Methods for process details and Supplementary Information and Supplementary Fig. 3 for the general design principles). First, the intended structure is designed and printed (step I) and a negative mould is made with a soft elastomer (step II). Here we used a commercial two-photon direct-write system to form the mould (Extended Data Fig. 2a) and crosslinked PDMS around it to form negatives (Extended Data Fig. 2b); note that ESCAPE is agnostic to how the mould and negative are fabricated. Liquid gallium is filled and solidified in the elastomer cavity and subsequently removed (or selectively etched) to generate the cast (step III). The gallium cast is then assembled into a device (Extended Data Fig. 2c) and the desired ECM is polymerized around it (step IV). Finally, gallium is liquified and evacuated using capillary forces (step V); phase-contrast images of the millimetre-scale Stanford bunny cavity are in Extended Data Fig. 2d. The empty cavity was used as a 3D cell-culture substrate in which human endothelial cells (ECs) were seeded to form a confluent lining to illustrate the final biological form of interest. Depth-coded projections of the cell nuclei are in Fig. 1e (top view) and Extended Data Fig. 2e (front view); Extended Data Fig. 2f shows cellular proteins F-actin (cytoskeleton) and VE-cadherin (cell–cell junctions). To evaluate patterning fidelity, we compared the collagen cavity (before cell seeding) with the original design (see Extended Data Fig. 2g) and observed that fine features such as the ear tips (about 50 μm) and the overall 3D body shape (about 1 mm) were accurately replicated.

Topologies such as tubes that split and remerge (for example, top design in Extended Data Fig. 3a) provide a distinct challenge for ESCAPE, as liquid gallium must break at each loop to be extracted (Extended Data Fig. 3b). Gallium was found to break reliably if the Laplace pressure of the collecting droplet (far left) is lower than the driving Laplace pressure. This is critical for evacuating topologies with closed loops in which the Laplace pressure decreases at junctions as one principal curvature approaches 0. Even dead-ended sections are evacuated reliably in hydrogels (in contrast to non-porous surrounding materials) as NaOH reaches the terminal sections of dead ends through the bulk (Extended Data Fig. 3c and Supplementary Video 6).

ESCAPE is compatible with other hydrogels, including fibrin and agarose (see Extended Data Fig. 3d,e and Supplementary Videos 7–9). We next sought to understand whether gallium exposure would lead to subsequent cytotoxicity to cells cultured after gallium removal. To assess this, we cultured human ECs in direct physical contact with gallium droplets for 4 days (Extended Data Fig. 3f). A live/dead assay (see Methods) showed no increased cell death and, furthermore, the cells grew directly on top of gallium (Extended Data Fig. 3g). Therefore, any potential traces of gallium remnant from ESCAPE (if present post long-term washing; see Methods) is expected to be non-cytotoxic. Post ESCAPE, collagen surfaces showed Ga residues <0.2% (atomic concentration) through energy-dispersive spectroscopy (EDS) and about 0.2% areal coverage through scanning electron microscopy (SEM) imaging (see Supplementary Fig. 4 and Methods).

To demonstrate the versatility of ESCAPE, we focus on vasculature as a use case, as the multiscalar diversity of vascular forms is a well-established fabrication challenge[11,12]. First, we developed a theoretical framework for capillary pumping in hierarchical vascular networks (Supplementary Information and Supplementary Fig. 5). Scaling relationships for capillary pressure, network impedance, evacuation flow rates and velocities show that natural branching laws favour liquid gallium evacuation through ESCAPE.

To establish a comparative baseline with standard needle moulding approaches for forming linear blood vessels[33], we cultured ECs under flow in 150-μm-sized ESCAPE-moulded tubes (see Extended Data Fig. 4a,b and Methods). The functionality of these vessels as measured by the endothelial barrier to transmural leakage is shown in Supplementary Fig. 6 (see Supplementary Video 10 and Methods). In smaller, 60-μm-sized vessels, fewer ECs are necessary to cover the vessel (Fig. 2a shows maximum projections of half a vessel). To assess the smallest vessels regions that are reliably covered by ECs, we designed a device tapering from 150 μm to 20 μm (about the size of an EC in suspension). ECs completely cover sections larger than 25 μm (Extended Data Fig. 4c) but coverage was incomplete at around 20 μm—the typical limit for seeding ECs in our devices.

In sinusoidal vessels (see Extended Data Fig. 4d and Fig. 2b), cells uniformly cover and align along both the linear and curved sections. Vessel architectures with symmetric (Fig. 2c) and asymmetric branching with dead ends exhibit uniform cell coverage (Extended Data Fig. 4e,f). We fabricated a design with a 150-μm parent vessel branching into three daughter vessels that each bifurcate and rejoin, and with calibres based on Murray's law[34,35]; see Extended Data Fig. 4g and design considerations in Supplementary Information and Supplementary Fig. 3d. The final vessel diameters closely match the intended design, with minor reductions from EC-generated contractile forces (Extended Data Fig. 4h,i). Gallium was evacuated successfully even with added constrictions in the smallest vessels (Extended Data Fig. 4j).

Complex interlocking geometries cannot be moulded in a single mould nor be printed in one pass with a nozzle, whereas multicomponent moulding and multipass printing result in interface defects. To make such traditionally 'non-mouldable' geometries such as an overhand knot achievable with ESCAPE, we designed thin continuous walls supporting the entire geometry (Extended Data Fig. 5a) while simultaneously ensuring that the wall thickness prevents high-surface-tension Ga from filling the supports (Extended Data Fig. 5b). The original knot, printed knot design, PDMS negative and Ga cast are shown in Extended Data Fig. 5c–f. The overhand knot formed in collagen can be endothelialized, demonstrating the ability of ESCAPE to generate topologically complex features (Fig. 2d and Extended Data Fig. 5g,h).

As well as overall vessel architecture, ESCAPE allows high-resolution control of vascular forms. To demonstrate this, we fabricated vascular malformations or spherical blebs extending from the cylindrical wall with varying offsets (Fig. 2e and Extended Data Fig. 6a). ESCAPE produces smooth collagen surfaces (without large ridges; Extended Data Fig. 6b) and sharp boundaries (collagen SHG slice in Extended

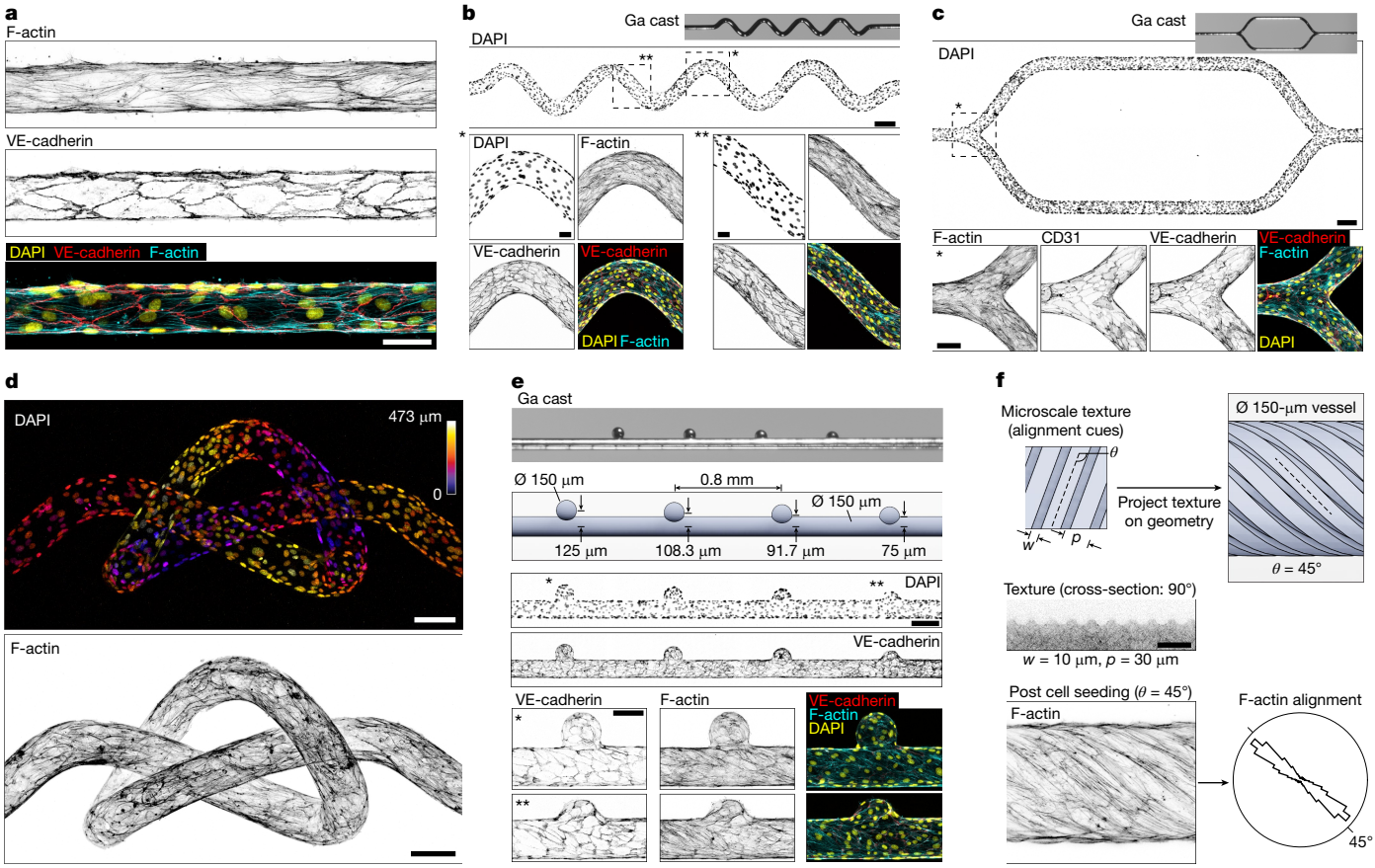

Fig. 2 | Endothelialized structures—vessel topologies and fine features. **a**, 60-µm cylindrical vessel. Scale bar, 50 µm. **b**, Sinusoidal vessel. Scale bar, 200 µm. See design in Extended Data Fig. 4. Close-ups show the curved and linear regions. Scale bars, 50 µm. **c**, 150-µm vessel that bifurcates into two equally sized daughter vessels. Scale bar, 200 µm. Zoomed-in sections show the branching junction. Scale bar, 100 µm. **d**, Geometries such as an overhand knot (100 µm diameter; see Extended Data Fig. 5) can be realized with the Ga ESCAPE moulding approach. Scale bars, 100 µm. **e**, Vascular malformations consisting of spherical blebs offset from the cylindrical vessel. Full device scale bar, 200 µm. Close-up projections scale bar, 100 µm. See volumetric views in Extended Data Fig. 6d. **f**, Microscale texture to orient ECs can be projected on the blood-vessel designs to control cell alignment as well as the overall vessel geometry. Images show the cross-section of the texture and a section of the vessel with grooves oriented at $\theta = 45°$ (see Extended Data Fig. 6e–g). Histogram shows the alignment of actin filaments in the cell. Scale bar, 50 µm.

Data Fig. 6c). Furthermore, ESCAPE enables tuning EC alignment within blood vessels—a well-established factor of vascular health and physiology[36]—which is challenging to achieve in 3D structures in natural ECMs. We introduced periodic microscale topographical cues (10-µm ridges) lining the vessel at various angles θ (Fig. 2f and Extended Data Fig. 6e) that control cell alignment precisely (histograms and images are in Extended Data Fig. 6f,g; see Methods).

Vascular trees

To highlight the fabrication of hierarchical architectures, we designed a range of branching vascular forms. First, we fabricated a five-level hierarchical tree with a ten times reduction in vessel calibre, for which each level consists of a parent branching into two dead-ended and one through branch (Fig. 3a and Extended Data Fig. 7a–c). The vessel calibres post cell seeding closely follow the original design (Extended Data Fig. 7d). Next, we designed a branching tree in which every vessel bifurcates into identical vessels, branching from one inlet into 32 perfusable outlets (Fig. 3b and Extended Data Fig. 7e,f; see cell alignments in Supplementary Fig. 7).

The previous vascular trees with calibres obeying Murray's law are orderly in a manner that natural vessels rarely are. We developed a custom version of the space colonization algorithm[37,38] to design more life-like vasculature (see Methods). Briefly, N virtual cells distributed randomly in a bounded space attract the growing branches of a tree until the branches come within a predefined distance (called vessel–cell distance (VCD)). Supplementary Fig. 8 shows dead-ended trees designed to nourish a 4 mm × 4 mm area generated using distinct design parameters that control the number and density of vessels, their tortuosity and overall alignment. Here we fabricated a design (N = 1,000, VCD = 100 µm) that terminates in 99 dead-ended branches (see Fig. 3c,d, Extended Data Fig. 8a,b and Supplementary Video 11); close-ups show branching regions and dead ends. Next, we synthesized a vascular tree in which the boundary to be vascularized is progressively expanded (to simulate organ growth) and fabricated the final design (see Fig. 3e and Extended Data Fig. 9a,b). As well as these mostly planar branching architectures, ESCAPE can create fully 3D hierarchical branching vascular trees following Murray's law, as shown in Fig. 3f and Extended Data Fig. 9c–h (see Methods).

Tissue architectures

As well as multiscalar vasculature, ESCAPE is applicable to other organotypic forms and engineered tissue architectures. Figure 4a shows an epithelial-cell-lined 3D ductal geometry with open lumens, designed to mimic natural epithelial branching (see Extended Data Fig. 10a,b). Next, we focused on a general design motif pervasive in many natural tissues in which independent networks weave through each other in proximity but never come in direct contact. Specifically inspired by the coordinated architecture of the lymphatic and

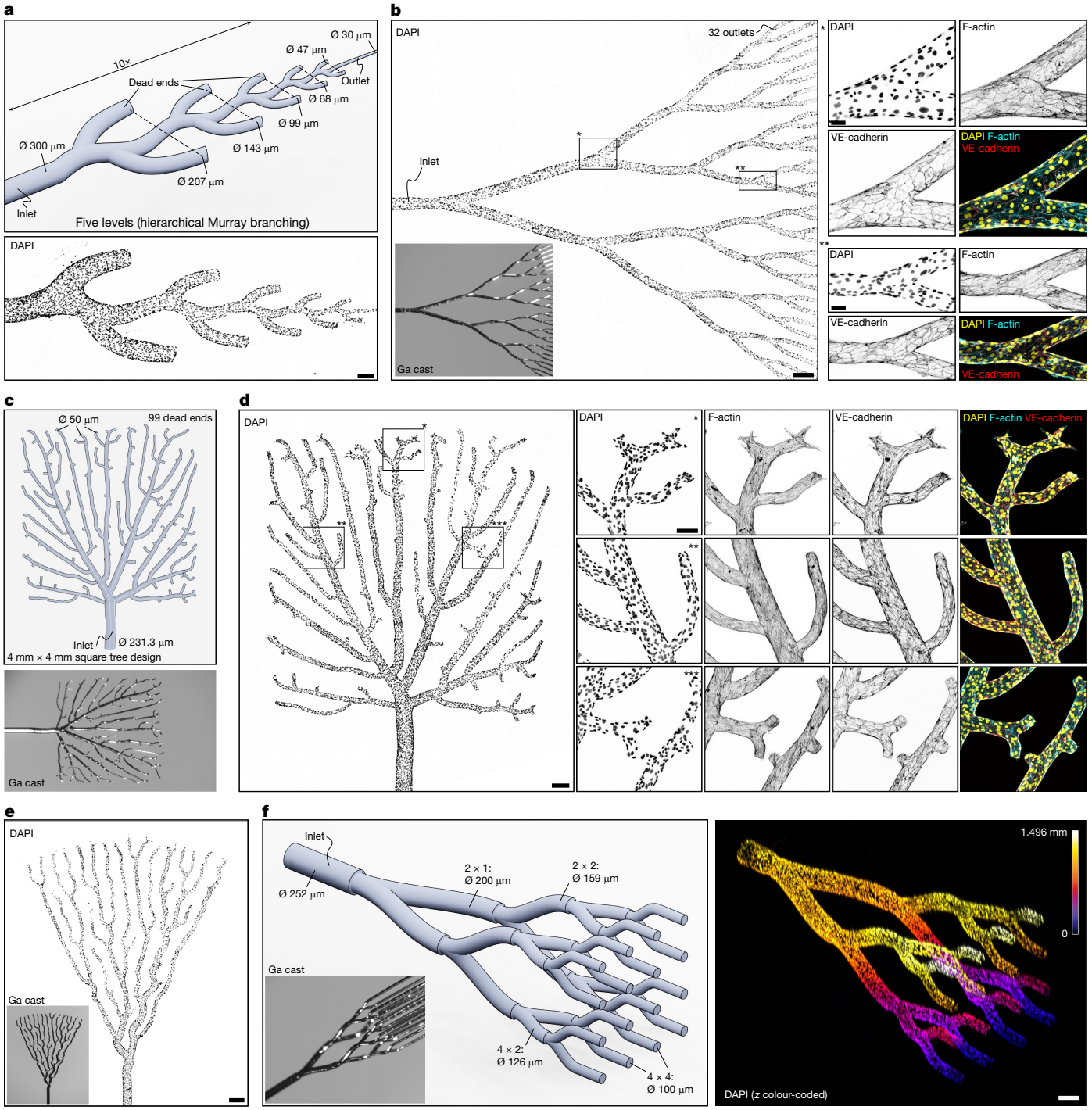

Fig. 3 | Hierarchical vascular trees and epithelial ducts. a, Hierarchical branching architecture with diameters spanning an order of magnitude. Scale bar, 200 µm. **b**, Tile scan of a binary branching tree in which each vessel is perfused (that is, the design has no dead ends). Scale bar, 250 µm. Inset, Ga cast. The close-up images show branching junctions at two hierarchical levels. Scale bar, 50 µm. **c**, Computationally generated square tree covering 4 mm × 4 mm. Each terminal branch of the tree is set to be a 50-µm-sized (dead-ended) vessel. All higher hierarchical branches are sized according to Murray's law, resulting in an inlet diameter of 231.3 µm. The tree was grown with a DOI of 1,000 µm and a VCD of 100 µm (see Supplementary Fig. 8 and Methods). Bottom image shows the Ga cast. **d**, Tile scan of the cell nuclei after cell seeding. Scale bar, 250 µm. The close-up images show portions of the device in which dead-ended sections come near each other and other regions of branching. Scale bar, 100 µm. **e**, Tile scan of a marginal growth tree (cell nuclei) designed to fit a sector of a circle, with aligned vessels. Scale bar, 250 µm. Inset, Ga cast. **f**, 3D branching vascular networks following Murray's law generated with ESCAPE. The design on the left shows four levels of branching starting from a single inlet to 16 perfused outlets in a 4 × 4 grid. Inset, Ga cast. 3D volume (right) shows the cell nuclei colour-coded by *z* value. Scale bar, 200 µm.

blood-vessel networks[39], we designed a dead-ended lymphatic network woven into a perfused, branching blood network (see Fig. 4b). To align the two distinct networks, we incorporated support structures that registered these Ga pieces at their ends, outside the gel region (Extended Data Fig. 10c,d; see Methods). Following ESCAPE and seeding the separate regions with blood and lymphatic ECs, confluent enmeshed dual 3D networks are formed (see Fig. 4c,d, Extended Data Fig. 10e–g and Supplementary Video 13). Next, to

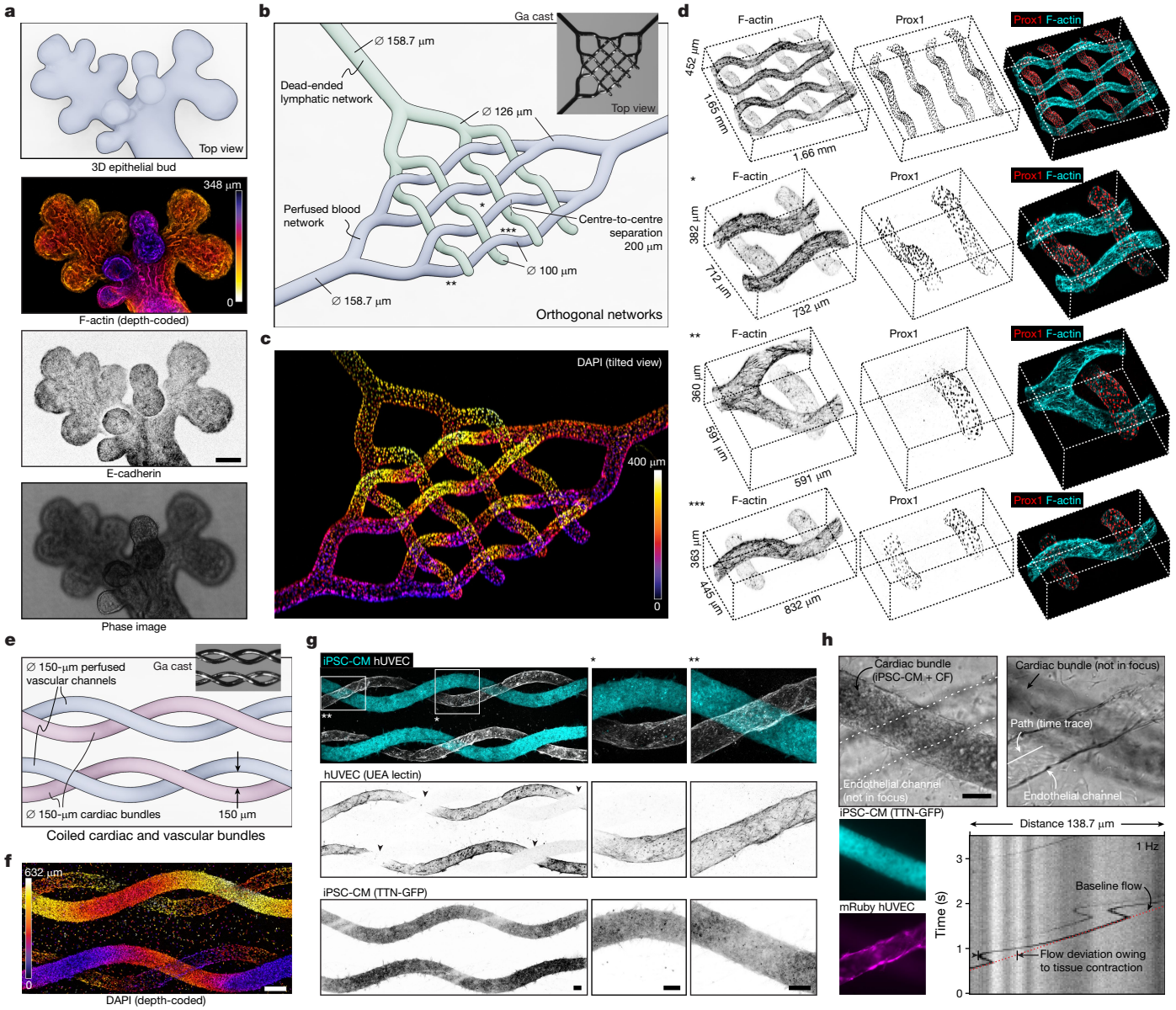

Fig. 4 | 3D applications of ESCAPE—epithelial ducts, multicellular orthogonal networks and cell-dense structures with proximal vasculature. a, The ESCAPE process can be expanded to non-vascular geometries such as epithelial ducts. Images show the original design of the 3D epithelial duct, depth-coded F-actin image, maximum projection of E-cadherin and a phase-contrast image post epithelial cell culture (see Extended Data Fig. 10a,b). Scale bar, 100 µm. **b**, Design of enmeshed blood (perfused) and lymphatic (dead-ended) networks and the resulting Ga cast. **c**, Cell nuclei colour-coded by *z* position showing the interwoven 3D geometry. **d**, Volumetric 3D view of the enmeshed regions showing all the cells (F-actin) and lymphatic cells (labelled by Prox1); corresponding DAPI images are in Extended Data Fig. 10f. **e**, Design of twisted cardiac and vascular bundles and corresponding Ga cast. **f**, The cardiac regions are maximally packed with iPSC-CMs (90%) and CFs (10%). The vascular conduits are lined by a confluent monolayer of ECs. The depth-coded DAPI image shows the helical cardiac bundles and vascular conduits. Scale bar, 200 µm. **g**, Tile scans and close-up images of the coiled section showing all cells, hUVECs (UEA lectin) and iPSC-CMs (TTN-GFP); corresponding DAPI images are in Extended Data Fig. 11i. Note that regions marked by arrowheads show a large drop in signal owing to the cell-dense cardiac region in the light path. Scale bars, 100 µm. **h**, Phase-contrast images focusing on both the cardiac bundle and the endothelialized vessel in the view, along with corresponding TTN-GFP and mRuby fluorescence images. Scale bar, 100 µm. Cardiac contractions displace the tracer beads added to the vascular channel as visualized through a kymograph recorded along a path (see Supplementary Video 16).

demonstrate the potential of ESCAPE in organizing a metabolically demanding tissue, we designed twisted pairs of 3D muscle bundles nourished by nearby vascular conduits (see Fig. 4e and Extended Data Fig. 11a,b). We first studied the contractile functionality of the cardiac bundles (maximally packed with 90% human-induced pluripotent stem-cell-derived cardiomyocytes (iPSC-CMs) and 10% cardiac fibroblasts (CFs); see Methods) alone without the ECs in the vascular conduits (Extended Data Fig. 11c,d). On electrical stimulation, the cardiac bundles contract, straining the surrounding matrix and affecting the flow profiles in the nearby vascular conduit, visualized by the flow of beads (see Extended Data Fig. 11e–g and Supplementary Videos 14 and 15). On subsequent endothelialization of the vascular conduit (Fig. 4f,g and Extended Data Fig. 11h,i), cell-dense 3D cardiac bundles with integrated vasculature are generated that feature contractile function (Fig. 4h and Supplementary Video 16).

Summary and conclusion

Biological function is closely tied to multiscalar forms that have largely remained challenging to engineer in natural materials. Here we present

a powerful new means to fabricate multiscalar shapes using gallium ESCAPE moulding. To aid the design process, we developed basic guidelines to form casts and extract them through capillary forces; in the future, gallium ESCAPE simulations can include efficient capillary withdrawal as a design metric. The ability to now achieve both micro-scale control of geometry as well as build hierarchical constructs opens new opportunities in the generation of an expansive set of organotypic designs and tissue architectures with built-in multiscalar vasculature.

Online content

Any methods, additional references, Nature Portfolio reporting summaries, source data, extended data, supplementary information, acknowledgements, peer review information; details of author contributions and competing interests; and statements of data and code availability are available at https://doi.org/10.1038/s41586-024-08175-5.

1. Weibel, E. R. It takes more than cells to make a good lung. *Am. J. Respir. Crit. Care Med.* **187**, 342–346 (2013).
2. Buckberg, G., Hoffman, J. I. E., Mahajan, A., Saleh, S. & Coghlan, C. Cardiac mechanics revisited: the relationship of cardiac architecture to ventricular function. *Circulation* **118**, 2571–2587 (2008).
3. Grigoryan, B. et al. Multivascular networks and functional intravascular topologies within biocompatible hydrogels. *Science* **364**, 458–464 (2019).
4. Lee, A. et al. 3D bioprinting of collagen to rebuild components of the human heart. *Science* **365**, 482–487 (2019).
5. Skylar-Scott, M. A. et al. Biomanufacturing of organ-specific tissues with high cellular density and embedded vascular channels. *Sci. Adv.* **5**, eaaw2459 (2019).
6. McKinnon, D. D., Brown, T. E., Kyburz, K. A., Kiyotake, E. & Anseth, K. S. Design and characterization of a synthetically accessible, photodegradable hydrogel for user-directed formation of neural networks. *Biomacromolecules* **15**, 2808–2816 (2014).
7. Brandenberg, N. & Lutolf, M. P. In situ patterning of microfluidic networks in 3D cell-laden hydrogels. *Adv. Mater.* **28**, 7450–7456 (2016).
8. Arakawa, C. K., Badeau, B. A., Zheng, Y. & DeForest, C. A. Multicellular vascularized engineered tissues through user-programmable biomaterial photodegradation. *Adv. Mater.* **29**, 1703156 (2017).
9. Daly, A. C., Prendergast, M. E., Hughes, A. J. & Burdick, J. A. Bioprinting for the biologist. *Cell* **184**, 18–32 (2021).
10. Pradhan, S., Keller, K. A., Sperduto, J. L. & Slater, J. H. Fundamentals of laser-based hydrogel degradation and applications in cell and tissue engineering. *Adv. Healthc. Mater.* **6**, 1700681 (2017).
11. O'Connor, C., Brady, E., Zheng, Y., Moore, E. & Stevens, K. R. Engineering the multiscale complexity of vascular networks. *Nat. Rev. Mater.* **7**, 702–716 (2022).
12. Traore, M. A. & George, S. C. Tissue engineering the vascular tree. *Tissue Eng. Part B Rev.* **23**, 505–514 (2017).
13. Truby, R. L. & Lewis, J. A. Printing soft matter in three dimensions. *Nature* **540**, 371–378 (2016).
14. Zheng, X. et al. Ultralight, ultrastiff mechanical metamaterials. *Science* **344**, 1373–1377 (2014).
15. Keating, S. J., Leland, J. C., Cai, L. & Oxman, N. Toward site-specific and self-sufficient robotic fabrication on architectural scales. *Sci. Robot.* **2**, eaam8986 (2017).
16. Xing, J.-F., Zheng, M.-L. & Duan, X.-M. Two-photon polymerization microfabrication of hydrogels: an advanced 3D printing technology for tissue engineering and drug delivery. *Chem. Soc. Rev.* **44**, 5031–5039 (2015).
17. Bellan, L. M. et al. Fabrication of an artificial 3-dimensional vascular network using sacrificial sugar structures. *Soft Matter* **5**, 1354–1357 (2009).
18. Kolesky, D. B., Homan, K. A., Skylar-Scott, M. A. & Lewis, J. A. Three-dimensional bioprinting of thick vascularized tissues. *Proc. Natl Acad. Sci. USA* **113**, 3179–3184 (2016).
19. Jiménez-Torres, J. A., Peery, S. L., Sung, K. E. & Beebe, D. J. LumeNEXT: a practical method to pattern luminal structures in ECM Gels. *Adv. Healthc. Mater.* **5**, 198–204 (2015).
20. Miller, J. S. et al. Rapid casting of patterned vascular networks for perfusable engineered three-dimensional tissues. *Nat. Mater.* **11**, 768–774 (2012).
21. Zheng, Y. et al. In vitro microvessels for the study of angiogenesis and thrombosis. *Proc. Natl Acad. Sci. USA* **109**, 9342–9347 (2012).
22. Lin, Y. et al. Vacuum filling of complex microchannels with liquid metal. *Lab Chip* **17**, 3043–3050 (2017).
23. Deng, F., Nguyen, Q.-K. & Zhang, P. Multifunctional liquid metal lattice materials through hybrid design and manufacturing. *Addit. Manuf.* **33**, 101117 (2020).
24. Hwang, D., Barron, E. J. III, Haque, A. T. & Bartlett, M. D. Shape morphing mechanical metamaterials through reversible plasticity. *Sci. Robot.* **7**, eabg2171 (2022).
25. Tang, S.-Y., Tabor, C., Kalantar-Zadeh, K. & Dickey, M. D. Gallium liquid metal: the devil's elixir. *Annu. Rev. Mater. Res.* **51**, 381–408 (2021).
26. Khan, M. R., Eaker, C. B., Bowden, E. F. & Dickey, M. D. Giant and switchable surface activity of liquid metal via surface oxidation. *Proc. Natl Acad. Sci. USA* **111**, 14047–14051 (2014).
27. Ma, J. et al. Shaping a soft future: patterning liquid metals. *Adv. Mater.* **35**, 19 (2023).
28. Pourbaix, M. *Atlas of Electrochemical Equilibria in Aqueous Solutions*. (NACE International, 1974).
29. Hardy, S. C. The surface tension of liquid gallium. *J. Cryst. Growth* **71**, 602–606 (1985).
30. Walker, G. M. & Beebe, D. J. A passive pumping method for microfluidic devices. *Lab Chip* **2**, 131–134 (2002).
31. Style, R. W., Jagota, A., Hui, C.-Y. & Dufresne, E. R. Elastocapillarity: surface tension and the mechanics of soft solids. *Annu. Rev. Condens. Matter Phys.* **8**, 99–118 (2017).
32. Bico, J., Reyssat, É. & Roman, B. Elastocapillarity: when surface tension deforms elastic solids. *Annu. Rev. Fluid Mech.* **50**, 629–659 (2018).
33. Polacheck, W. J., Kutys, M. L., Tefft, J. B. & Chen, C. S. Microfabricated blood vessels for modeling the vascular transport barrier. *Nat. Protoc.* **14**, 1425–1454 (2019).
34. Murray, C. D. The physiological principle of minimum work. *Proc. Natl Acad. Sci. USA* **12**, 207–214 (1926).
35. Sherman, T. F. On connecting large vessels to small. The meaning of Murray's law. *J. Gen. Physiol.* **78**, 431–453 (1981).
36. Wang, C., Baker, B. M., Chen, C. S. & Schwartz, M. A. Endothelial cell sensing of flow direction. *Arterioscler. Thromb. Vasc. Biol.* **33**, 2130–2136 (2013).
37. Runions, A. et al. Modeling and visualization of leaf venation patterns. *ACM Trans. Graph.* **24**, 702–711 (2005).
38. Runions, A., Lane, B. & Prusinkiewicz, P. in *Proc. 3rd Eurographics Workshop on Natural Phenomena (NPH'07)* (eds Ebert, D. & Mérillou, S.) 63–70 (Eurographics Association, 2007).
39. Oliver, G., Kipnis, J., Randolph, G. J. & Harvey, N. L. The lymphatic vasculature in the 21st century: novel functional roles in homeostasis and disease. *Cell* **182**, 270–296 (2020).

Methods

Materials

PDMS was prepared by mixing Sylgard 184 base with the curing agent at 10:1 ratio (SYLGARD 184 Silicone Elastomer Kit, Dow), degassed and cured in an oven at 60 °C for more than 2 h (typically overnight). Gallium was used as purchased (50-g tubes, CAS 7440-55-3, Luciteria Science). Solutions of NaOH were prepared by serial dilution from a 5N solution (Sodium Hydroxide 5N, #SS256-500, Thermo Fisher Scientific) with ultrapure water (Milli-Q, Direct-Q UV Remote Water Purification System, MilliporeSigma). Collagen gels (2.5 or 4 mg ml^{-1}) were prepared from high-concentration 8–11 mg ml^{-1} rat tail collagen I stocks (#354249, Collagen I, High Concentration, Rat Tail, Corning) based on a general protocol for forming 3D collagen gels[40]. Briefly, collagen was buffered with a 10× reconstitution buffer (10× RB is made of 2.2 g sodium bicarbonate and 4.8 g HEPES in 100 ml distilled water) and 10× DMEM (#D2429, Sigma-Aldrich), titrated to a pH of 9 with 1 M NaOH and diluted with phosphate-buffered saline (PBS) to a final concentration (2.5 or 4 mg ml^{-1}), all in an ice bucket. This pre-gel solution was injected into chambers as desired and left to polymerize overnight at room temperature (RT) in a humid atmosphere to prevent evaporation. Fibrin gels were formed by first dissolving fibrinogen from bovine plasma (#F8630, Sigma-Aldrich) at a concentration of 5 mg ml^{-1} in DPBS (#14287080, Thermo Fisher Scientific) at 37 °C and sterile filtering (0.2-µm filter). The fibrinogen solution was mixed with thrombin (#T4648, Sigma-Aldrich) at a ratio of 0.1 U of thrombin per mg of fibrinogen and immediately injected into desired regions and left to clot. Agarose gels were formed by dissolving 5% w/v of ultralow-gelling-temperature agarose (#A5030, Sigma-Aldrich) in PBS at 60 °C. Before injection, the devices were cooled (optional) and agarose was injected into the devices as the solution was cooling.

Cell culture

Human microvascular blood ECs (dermal hMVECs; #CC-2813, Lonza) were cultured and maintained in Microvascular Endothelial Cell Growth Medium-2 (EGM-2MV media: EBM-2 basal media (Lonza) supplemented with the MV2 BulletKit). Human umbilical vein endothelial cells (hUVECs; #C2519A, Lonza) were cultured and maintained in EGM-2 media (Lonza). hMVECs and hUVECs were used at passages 4–6. LifeAct-Ruby-hUVECs (mRuby-hUVECs) were generated and described in a previous study[41] and cultured in EGM-2 media. Human epithelial cells (colorectal adenocarcinoma cells, Caco-2; ATCC) were cultured and maintained in a medium containing DMEM/F-12 (#11320033, Thermo Fisher Scientific) supplemented with 10% FBS (#F0926, Fetal Bovine Serum, Sigma-Aldrich) and 1% v/v penicillin–streptomycin (Invitrogen). Dermal lymphatic ECs (pooled human dermal microvascular ECs; mixed population of blood and lymphatic ECs, #CC-2516, Lonza) was used as the source of lymphatic ECs. Lymphatic ECs (Prox1-positive) were cultured and maintained in EGM2-MV and were used at passages 4–6. Human ventricular CFs (#CC-2904, Lonza) were cultured and maintained in Cardiac Fibroblast Growth Media (FGM-3; #CC-4526, Lonza) and used at passages 4–7. iPSC-CMs were differentiated from an iPSC line (PGP1 parent line subclone with green fluorescent protein (GFP) tagged to endogenous titin (TTN)) manipulating the Wnt signalling pathway using previously reported methods[42,43]. Briefly, iPSCs under monolayer culture (RPMI medium with B27 minus insulin; Thermo Fisher Scientific) were first Wnt-activated using 12 µM CHIR99021 (#4423; Tocris Bio-Techne) on day 0 for 24 h and then Wnt-inhibited using 5 µM IWP4 (#5214; Tocris Bio-Techne) on day 3 for 48 h. On day 9, cells were switched to culture in RPMI medium with B27 with insulin (Thermo Fisher Scientific) and underwent metabolic selection on day 11 in 4 mM sodium DL-lactate in glucose-free RPMI (Thermo Fisher Scientific) for 4 days. After metabolic selection, iPSC-CMs were replated onto fibronectin-coated 12-well plates (10 µg ml^{-1} fibronectin; #356009; Fisher Scientific) and maintained in RPMI supplemented with B27 with insulin for at least 2 weeks (day 30+) before use in experiments. All cells were maintained at 37 °C in 5% CO_2 in humidified incubators.

Antibodies and reagents

Anti-VE-cadherin (F-8, 1:500 dilution) was from Santa Cruz (#sc-9989, Santa Cruz). Anti-VE-cadherin (D87F2, 1:500 dilution, #2500S) and Anti-E-cadherin (24E10, 1:1600 dilution, #3195S) were from Cell Signaling Technology. Phalloidin conjugated with Alexa Fluor 488 (#A12379), phalloidin conjugated with Alexa Fluor Plus 555 (#A30106) and phalloidin conjugated with Alexa Fluor Plus 647 (#A30107) were purchased from Invitrogen/Thermo Fisher and prepared as a DMSO stock solution (about 66 µM) and used at 1:1,000 dilution. Anti-Prox1 (#102-PA32, 1:500 dilution of 0.5 mg ml^{-1} stock) primary was from ReliaTech. Ulex Europaeus Agglutinin (UEA lectin) DyLight 649 (1:250 dilution) was from Vector Labs (#DL-1068-1). Anti-mouse and anti-rabbit secondary antibodies with Alexa Fluor Plus 488, 555 and 647 (#A32790, #A32773, #A32733) and DAPI (#D3571) were from Invitrogen/Thermo Fisher and used at 1:1,000 dilution. LIVE/DEAD Viability/Cytotoxicity Kit for mammalian cells was purchased from Invitrogen/Thermo Fisher (#L3224) and used following the manufacturer's recommended protocol.

Ga adhesion experiments

12-mm-wide holes were punched out of approximately 0.25″ thick slabs of PDMS. PDMS pieces and glass coverslips were then plasma cleaned at 100 W for 30 s (EMS Quorum 1050X, Electron Microscopy Sciences) and bonded together to form wells. For PDMS–Ga adhesion experiments, the internal surfaces of the wells were coated with freshly mixed 10:1 PDMS (monomer:crosslinker) and cured at 100 °C for at least 1 h. For PDMS–agarose adhesion experiments, a layer of freshly prepared 5% w/v of ultralow-gelling-temperature agarose (#A5030, Sigma-Aldrich) in PBS was added to the bottom of the wells, sealed with tape to prevent evaporation and gelled at 4 °C for 1 h. Beads of liquid Ga (about 3 mm) were added to wells with freshly prepared PDMS or agarose gels, respectively, and left overnight to form an oxide layer and stabilize their interface with the underlying substrate. When low concentrations of NaOH (10 mM) was added to stabilized liquid Ga droplets on agarose substrates, the Ga droplets quickly formed spheres and were easily dislodged (<10 s) on tilting. However, with 10 mM NaOH exposure, Ga droplets on PDMS substrates lost the oxide layer and turned shiny in the same period (as previously described[44]) but remained adhered (Supplementary Fig. 1 and Supplementary Video 1). To quantify the adhesion between Ga and PDMS, these wells with stable liquid Ga drops were filled with different concentrations of NaOH, covered with a glass coverslip and flipped. When the oxide layer was fully removed and the hanging droplets of liquid Ga detached from the PDMS, they formed spheres and dropped down (see Supplementary Video 1); the time to detach is quantified in Supplementary Fig. 1b. Overall, Ga adheres to PDMS much more strongly than water-based gels and requires high concentrations of NaOH (about 1 M) to detach from PDMS in minutes.

Ga filament fabrication

150-µm-diameter cylinders were designed in a computer-aided design (CAD) software package (SolidWorks, Dassault Systèmes) and printed on pre-treated silicon substrates. To prepare silicon substrates for printing, they were plasma cleaned at 100 W for 30 s (EMS Quorum 1050X, Electron Microscopy Sciences) and left overnight in a vacuum desiccator with 20 µl of 3-(trimethoxysilyl) propyl acrylate (#475149 Sigma-Aldrich, MilliporeSigma). The design was printed on the treated silicon substrate using a commercial two-photon direct laser writing system (Photonic Professional GT, Nanoscribe) with a 25× objective with the photoresist IP-Dip (Nanoscribe). The printed parts were cleaned in polyethyl glycol mono ether acetate (PGMEA; #484431, Sigma-Aldrich) for 30 min to remove uncured resist and rinsed with isopropanol (IPA), followed by Novec 7100 (3M Company) and left to dry for more than 2 h. To make the printed mould non-adhesive in subsequent steps,

the part was plasma cleaned for 100 W at 30 s and silanized for 3 h in a vacuum desiccator with trichloro(1H,1H,2H,2H-perfluorooctyl)silane (#448931, Sigma-Aldrich). The negative copy of the shape was formed by polymerizing PDMS around the structure. Gallium was melted at 45 °C and injected into the cylindrical void, after which it was solidified and extracted from within the PDMS to form a free-standing Ga filament.

Ga filament evacuation

To first test the ESCAPE process with linear Ga filaments, the filaments were assembled into a PDMS device consisting of a 6-mm-wide chamber (Fig. 1a). The PDMS devices with chambers were fabricated from negative moulds (designed in SolidWorks) and printed commercially (Protolabs). PDMS chambers and glass coverslips were plasma cleaned at 100 W for 30 s and allowed to cool briefly, after which they were bonded together after placing the Ga filaments to span the chamber. The devices were left to sit overnight at RT and were cleaned with ethanol. To prepare the internal surface of the PDMS chambers for gel attachment, the assembled chambers were treated with a 0.5 mg ml^{-1} solution of dopamine hydrochloride in tris-buffered saline (diluted from 10× Tris Buffered Saline, #T5912, Sigma-Aldrich, and adjusted to a pH of 8.5 with a 5 N NaOH solution) for 1 h. After this, the devices were rinsed in deionized water, followed by 50% ethanol (in deionized water) and ethanol and left to dry in a vacuum chamber for 2 h. Alternatively, the chambers could be treated with poly-L-lysine (PLL) followed by glutaraldehyde to promote collagen binding, as described previously[33]. After surface treatment and drying, 2.5 mg ml^{-1} collagen pre-gel solution was prepared as described in the 'Materials' section and injected into the gel chambers and left to polymerize overnight at RT in a humid environment. The next day, until gallium evacuation, to prevent any evaporation of water from the gel, PBS was added to the reservoirs at both ends of the chambers. To begin evacuation, devices were placed on a hotplate (Benchmark) set to 32 °C; the melting of Ga filaments can be observed typically within 2–5 min. Then the extra PBS previously added to the end reservoirs were removed and replaced with NaOH solution of the desired concentration; the right reservoirs were filled with more liquid to create a pressure head for NaOH solution to reach the evacuating end. Images were captured every 2 s (Canon EOS 6D Mark II with macro lens Canon EF 180mm f/3.5L Macro USM) and made into a time-lapse at 30 frames per second (FPS). For the 10 mM NaOH condition in Fig. 1b, fresh 10 mM NaOH solution was added once at the 11-min mark to re-establish the pressure head.

SHG characterization of collagen

To study the dimensional stability of collagen cavities on exposure to NaOH solutions, needle-moulded collagen gels were first formed. 4 mg ml^{-1} collagen gels (as described in the 'Materials' section) were polymerized in surface-treated PDMS chambers (see the 'Ga filament evacuation' section for the treatment procedure) around 160-µm-sized needles (that were pre-soaked in 0.1% bovine serum albumin solution for 1 h; prepared from #A2058, Bovine Serum Albumin, Sigma-Aldrich). Following overnight gelling, the needles were removed, leaving cylindrical conduits of 160 µm diameter (Extended Data Fig. 1a). The two reservoirs connecting the cylindrical channel were filled with a total volume of 75 µl of PBS (control), 10 mM, 20 mM, 50 mM or 100 mM NaOH solutions with a pressure head to cause flow through the channel and placed on a hotplate at 32 °C for 30 min. Following this, the devices were removed and rinsed in PBS three times. Collagen architecture was analysed through SHG images that were obtained with a Leica TCS SP8 MP Multiphoton Microscope equipped with a tunable (680–1,300 nm) fs laser (InSight DeepSee, Spectra-Physics) set to 885-nm excitation. The SHG signal was recorded with the HyD-RLD two-channel detector (non-descanned detection) with the SHG 440 filter cube (BP 440/20 nm and BP 483/32 nm filters) using the HC FLUOTAR L 25×/0.95 and HC APO L U-V-I10×/0.3 water immersion objectives. The dimensions of the vessel were measured using ImageJ; first, the central slice of the volumetric stack was identified and the lumen size was measured from the central slice. For bulk collagen intensity measurement (Extended Data Fig. 1d), 5-mm-wide circular wells were punched out of approximately 1-mm-thick PDMS sheets that were then bonded to a glass coverslip. 25 µl of 4 mg ml^{-1} collagen was added to each well and polymerized overnight as described previously, forming approximately 1-mm-thick collagen gels. These gels were submerged in different concentrations of NaOH for 30 min at 32 °C, after which they were rinsed in PBS and imaged. Averaged intensity profiles in Extended Data Fig. 1b and bulk average collagen SHG intensity in Extended Data Fig. 1d were computed using MATLAB (MathWorks).

General ESCAPE process

First, the intended geometry was designed using constructive solid geometry using interactive CAD tools (SolidWorks) or procedural CAD modellers such as OpenSCAD (http://openscad.org/) and Blender 2.91 (Blender Foundation). The geometries were designed on the basis of the design criteria described in the Supplementary Information. A version of the original Stanford bunny model (http://graphics.stanford.edu/data/3Dscanrep/#bunny) was downloaded from https://github.com/dcoeurjo/VolGallery/tree/master/Stanford-bunny and used for Fig. 1d,e and Extended Data Fig. 2. For generating the initial moulds in this work, a two-photon direct laser writing system (Photonic Professional GT, Nanoscribe) was used with a 25× objective with the photoresists IP-Dip and IP-S (Nanoscribe). Following the approach in the 'Ga filament fabrication' section, the printed moulds were cleaned, surface treated with tri chloro(1H,1H,2H,2H-perfluorooctyl)silane and PDMS was crosslinked around the mould to make the negative structure. For most designs, a PDMS monomer to crosslinker ratio of 10:1 was used (except for some 3D designs, such as the Stanford bunny design and 3D branching vascular network design, in which a 20:1 ratio was used to make a softer PDMS). The gallium cast was formed by placing molten gallium on top of a cavity, forming a sealed enclosure and applying and releasing vacuum. In designs with small features, on releasing vacuum, the PDMS negative with infilled gallium was placed on a hotplate and more pressure was applied manually for liquid gallium to reach the smallest regions (see Supplementary Information and Supplementary Fig. 3 for a discussion of the criteria). The excess gallium was then removed with a wipe soaked in ethanol and the PDMS negative with infilled gallium was cooled to 4 °C, after which the supercooled liquid Ga was brought in contact with a crystalline structure to initiate solidification. The solid gallium cast was typically separated from the PDMS negative by peeling the PDMS after solidifying the Ga cast. In designs such as the overhand knot (Fig. 2d), 3D hierarchical tree (Fig. 3f), orthogonal networks (Fig. 4b) and cardiac bundles (Fig. 4e), in which the PDMS negative cannot be removed without deforming the solid Ga cast, the PDMS negative was etched using a selective etch. A 1:4 ratio of 1 M tetrabutylammonium fluoride (TBAF) in tetrahydrofuran (#216143, Sigma-Aldrich) to acetone was used to etch PDMS; acetone was used as a solvent because of its low swelling index and also because the combination of TBAF and acetone yielded a high etch rate[45]. The duration of the etch was typically under an hour and was timed on the basis of the size of PDMS to be etched. The Ga cast was rinsed in ethanol and then left to dry. Typically, Ga casts were assembled into PDMS devices with chambers to hold the soft gel. PDMS chambers and glass coverslips (24 mm × 30 mm, No. 1, #48393-092, VWR) were cleaned in a plasma asher (EMS Quorum 1050X, Electron Microscopy Sciences) for 30 s at 100 W and left to cool for 1–2 min. The PDMS devices were bonded to the glass coverslips with the Ga cast inside and left to bond overnight. The assembled chambers were treated with 0.5 mg ml^{-1} dopamine hydrochloride in tris-buffered saline for 1 h, rinsed in deionized water, followed by 50% ethanol and ethanol and left to dry in a vacuum desiccator for 2 h as described in the 'Ga filament evacuation' section. After this, the soft gel material of choice (agarose, collagen or fibrin) was injected into the gel chambers around the Ga cast and left to

gel following the description in the 'Materials' section. PBS was added to the devices to prevent evaporation of the hydrogels post gelling. To evacuate the Ga cast, the PDMS devices were placed on a hotplate at 32 °C to first melt the Ga cast. The process was monitored continuously using a stereo microscope (ZEISS SteREO Discovery V20 Motorized Stereo Microscope, Carl Zeiss). Typically, 10 mM NaOH was used to remove the surface oxide of gallium (unless noted otherwise); a fluidic pressure head was created from the retracting end to the collecting end to ensure that NaOH solution reached all parts of the devices through the bulk interstitial space to remove the surface oxide of gallium. The pressure head was restored (approximately every 10–15 min) with fresh NaOH solution to ensure flow through the gel interstitial space. After complete gallium evacuation, the gallium droplets collected in the reservoirs were removed and the gels and reservoirs were washed with PBS three times. After inspecting the devices in the stereo microscope, fresh PBS was added to the reservoirs with a pressure head to ensure flow through the cavities and the gels, after which the devices (soaked in PBS) were stored at 4 °C overnight. At this stage, all NaOH is considered to be fully washed out from the gel; the measured pH is the same as that of PBS.

General device seeding and culture

The PDMS devices with the soft gels after gallium evacuation through ESCAPE were stored with PBS in the reservoirs at 4 °C. The night before cell seeding, the devices were brought to RT and the PBS was removed from the reservoirs and the gel regions. 50 µl of fresh cell-culture media depending on the intended cell type (for example, EGM-2MV for hMVECs) was added to each media reservoir. The devices were then transferred to a rocker inside a tissue culture incubator (humidified; 37 °C with 5% CO_2) for at least 4 h (typically overnight). On the day of cell seeding, cells were lifted from cell-culture dishes with 0.05% trypsin/EDTA (Gibco) and centrifuged at 200 g for 4 min. Cells were then resuspended in the growth medium at a density of 1×10^6 cells ml^{-1} (counted with a haemocytometer). In total, 50–70 µl of cell suspension was added across the two reservoirs for the cells to flow into the gel conduits; devices were occasionally flipped and turned for cells to reach different parts of the conduits (over the course of about 5 min), after which the devices were stored in the incubator for 15–30 min for the cells to attach. Following this, the excess cell solution was removed from the reservoirs and 50 µl of cell-culture media was added to each reservoir and the devices were placed on a rocker in the incubator. Culture medium was changed daily and the devices were observed through a bright-field microscope for cell confluence; typically, full confluence was achieved 2–3 days after seeding.

Immunofluorescence and microscopy

Devices containing cell-lined vessels and cavities were fixed with a 4% paraformaldehyde (Electron Microscopy Sciences) in PBS for 15–30 min. Devices were then washed with PBS and permeabilized with 0.15% Triton X-100 (Sigma-Aldrich) for 15–30 min at RT in the presence of a pressure head to ensure that solution reached all areas of the device. The devices were then blocked with 3% BSA for 1 h at RT (or overnight at 4 °C). The devices were then washed in PBS thrice and primary antibodies and phalloidin in 3% BSA (at the respective dilutions stated in the 'Antibodies and reagents' section) were added to the device and left overnight at 4 °C. Next, the devices were washed two times in PBS and fresh PBS was added to the device ports and left at 4 °C in the presence of a fluidic pressure head for 2 h. The solution was then replaced with the secondary antibodies in 3% BSA and stained overnight at 4 °C. The next day, the devices were washed three times in PBS and cell nuclei were marked with DAPI for 1 h, after which the devices were washed in PBS. Immunofluorescence images of the devices were obtained using a Leica TCS SP8 MP multiphoton microscope with the HC FLUOTAR L 25×/0.95 and HC APO L U-V-I 10×/0.3 water immersion objectives. Tile scans were controlled and obtained at constant laser intensity using the LAS-X software (Leica). Images were adjusted uniformly for contrast and brightness using ImageJ. ImageJ was also used to generate composite images, z projections, depth-coded images and stitch tile scans. 3D volumetric views of the vascular malformation (Extended Data Fig. 6d) were generated with Imaris 9.7.2 (Oxford Instruments). Bright-field images (Extended Data Figs. 2b,d, 5e and 6b) were acquired using a Nikon Eclipse TE200 microscope. SEM images were acquired with a Field Emission Scanning Electron Microscope Zeiss Supra 55VP (Carl Zeiss); before SEM imaging, samples were optionally surface coated with Au/Pd using a Cressington 108 sputter coater.

Comparing ESCAPE in porous hydrogels versus non-porous materials

To compare the effectiveness of the ESCAPE process in conduits in hydrogels and non-porous materials, we used the design of a vessel that branches into two daughter vessels, one of which is dead ended (Extended Data Fig. 3a, bottom). Ga casts were formed as previously described and assembled into PDMS devices with chambers to hold the gels. 5% agarose was used as the porous gel and PDMS was used as the non-porous material. Gallium evacuation was performed with 10 mM NaOH in the agarose gel. Because gallium adheres to PDMS more than water-based gels, and with PDMS being more hydrophobic, a high concentration of NaOH (100 mM) was used for switching the surface tension of gallium.

Live/dead assay

The effects of culturing cells in direct contact with gallium were evaluated by adding roughly 5-mm-sized droplets of gallium into the centre of the wells in a six-well plate. Culture media was added and pre-warmed in these wells, following which hMVECs and hUVECs were seeded at low confluence (about 20%) and cultured for 4 days. Cell-culture medium was changed once 2 days after cell seeding. The live/dead assay was performed using the cell viability kit (see the 'Antibodies and reagents' section) following the recommended protocol and imaged from the top using the Leica TCS SP8 MP Multiphoton Microscope.

Characterization of Ga remnants—EDS analysis and particle counting

A mould geometry with four vertical posts (see Supplementary Fig. 4a) was used to generate collagen structures (4 mg ml^{-1}) using the full ESCAPE process. The solvent in these hydrated collagen samples was gradually switched out from PBS to ethanol (through soaking in 25%, 50%, 70%, 80% and 90% ethanol intermediates for 30 min each). Finally, the samples were left overnight in pure ethanol and then critical point drying was performed (SAMDRI Manual Critical Point Dryer, tousimis). Collagen surfaces in direct contact with Ga before Ga evacuation were inspected post-ESCAPE for Ga residues through EDS analysis (Phenom ProX Desktop SEM with EDS; Thermo Fisher Scientific) with an accelerating voltage ≥10 kV. Elemental maps showed spherical residues to Ga (Supplementary Fig. 4b) on exposed collagen surfaces corresponding to 0.18% (atomic concentration) through regional analysis (Supplementary Fig. 4c). To account for environmental contaminants that potentially underreport the amount of Ga, we carried out spot analysis on Ga residues (that ideally must report 100% Ga). These spots reported 69.8% (atomic concentration) Ga; the remaining fraction is considered as contaminants (Supplementary Fig. 4d,e). Second, to calibrate for noise in measurements that potentially result in overreporting the amount of Ga, we carried out spot analysis on collagen surfaces that were never in contact with Ga and found 0.10% (atomic concentration) Ga. Using these two calibrations, the adjusted Ga residue is 0.11% (atomic concentration). In summary, the total Ga residues are measured as 0.11% (atomic concentration; corrected) or 0.18% (atomic concentration; uncorrected) as measured through EDS. Next, 13 samples were analysed through SEM imaging and particle counting (ImageJ). The microscale particulates covered 0.2% of the total imaged area (Supplementary Fig. 4f).

Diffusive permeability measurement

Linear vessels (150 μm diameter) were fabricated using the general ESCAPE process in 4 mg ml^{-1} collagen. For the cell-lined vessel group, hMVECs were seeded into the channels and cultured for 3 days until a confluent monolayer was formed. A group of empty vessels (that is, without ECs) was prepared simultaneously as the control. Both groups of devices were cultured on a rocker inside a tissue culture incubator (humidified; 37 °C with 5% CO_2) before the vascular barrier measurement. To assess the vascular barrier function of ESCAPE-fabricated vessels, a previously reported protocol to measure diffusive permeability was used[33]. Briefly, devices were removed from the rocker and brought to an environment-controlled confocal microscope (humidified; 37 °C with 5% CO_2). The vessel was aligned in bright field such that the entire width of the vessel was visible near the bottom of the imaging area and a large portion of the bulk gel on one side was visible on top. Focus was adjusted to the widest region of the vessel and 50 μl of 70-kDa fluorescent dextran (Dextran, Texas Red, #D1830, Thermo Fischer Scientific) diluted to 12.5 μg ml^{-1} in PBS was added to one of the media ports. Fluorescent dextran flowing through the vessel and diffusing into the gel region were imaged in each frame (150 frames; 5-s interval between frames; see Supplementary Video 10). The vessel was manually segmented for each device to then define the vessel and bulk gel area in MATLAB. The diffusive permeability coefficient was then calculated as $P_D = (2r/I_0)\frac{dI}{dt}$, in which r is the radius of the vessel, I_0 is the fluorescent intensity in the vessel region and I is the fluorescent intensity in the bulk gel region (Supplementary Fig. 6). Compared with empty collagen vessels (that is, with no cell lining; control) with mean $P_D = 51.6 \times 10^{-6}$ cm s^{-1}, cell-lined vessels had substantially reduced diffusive permeability $P_D = 12.2 \times 10^{-6}$ cm s^{-1} (or stronger vascular barrier), as measured across 15 devices per condition.

Quantifying actin alignment

From the volumetric images of the vessels, the central slice was identified in ImageJ and the maximum z projection of one half of the vessel was obtained. The maximum z projection of the entire vessel was used when a single image slice did not separate the entire imaged region into two clear halves. The following automated approach was used to quantify the overall alignment of actin filaments in the vessels with the topographical cues (Fig. 2f, Extended Data Fig. 6e–g and Supplementary Fig. 7). The F-actin channel of the maximum z-projection images were loaded in MATLAB and a 20-μm-long structuring element (angle iteratively varied from 0° to 360° in 1° increments) was used to perform a morphological opening of the image. From the central part of the vessel, the pixels in the actin image with a high degree of alignment were automatically estimated from the morphological opening intensities. The peak alignment direction was recorded from these regions and a polar histogram was generated to highlight the orientation of the actin bundles.

Deterministic branching vascular tree designs

The branching tree with five hierarchical levels with two dead-ended branches and one through branch at each level (Fig. 3a) was designed procedurally in OpenSCAD such that Σr^n is conserved, in which the exponent $n = 3$ in ideal Murray's law. For the design in Fig. 3a, an exponent of $n = 2.96$ was used to demonstrate that n can be varied in design easily. The fully perfusable branching tree design in Extended Data Fig. 7e with one inlet and 32 outlets and the 3D branching tree (Fig. 3f) with one inlet and a 4 × 4 array of outlets were generated using the Blender Python API (Blender Foundation). The vessel calibres were based on the ideal Murray's law exponent $n = 3$.

Design of space colonization trees

Computationally designed vascular trees were generated on the basis of our custom implementation of the space colonization algorithm[37,38] in Blender with the Python API. Briefly, a set of N virtual cells (or attractors) were randomly distributed within a specific boundary. For the results in Supplementary Fig. 8, the boundary was defined to be a 4 mm × 4 mm square region. The starting node of the tree was defined to be near (or inside) this boundary. The tree is grown iteratively such that all the cells are 'nourished', that is, within a predefined VCD from the branches of the vascular tree; this is analogous to living cells being within a diffusion length away from blood vessels in natural tissues. In each iteration, virtual cells that are within a predefined distance of influence (DOI) but not nourished by the vascular tree (that is, not within VCD from any of the branches of the tree) attract the node closest to them. Cells outside the DOI are treated to be too far to influence the tree growth. New segments of the tree are added from all of the nodes attracted by cells towards the average direction of all cells attracting that specific node (the growth vector); random noise and tortuosity factor are optionally added to the growth vector in this step of the algorithm to make the vessel segments tortuous. Step size is the spacing between the nodes during the tree growth. This process is continued until all of the cells are within VCD from the tree (or a maximum number of iterations is reached) and yields a tree skeleton. The generated tree skeleton is automatically cleaned to remove single segment branches. After clean-up, the tree skeleton is sized according to natural scaling laws law starting with the terminal branches of the tree; for example, in Supplementary Fig. 8, the terminal branches are designed to have a radius of 25 μm and all parent vessels are sized such that Σr^3 is conserved. The vascular tree fabricated using ESCAPE (Fig. 3c,d and Extended Data Fig. 8) was generated with the following parameters: 4 mm × 4 mm boundary, $N = 1{,}000$ cells, DOI = 1,000 μm, VCD = 100 μm, step size = 50 μm, radius of terminal vessels = 25 μm; Supplementary Video 11 shows the growth of the tree through the different iterations.

In the above examples, the overall boundary was fixed throughout the iterations. To simulate organ growth, the boundary of the vascular tree can be expanded each iteration as desired, at a defined growth rate (called marginal growth). The marginal growth tree design in Extended Data Fig. 9a and Fig. 3e was generated using the sector of a circle (with sector angle 53.1°) as the boundary but whose radius was grown at a rate of 12.5 μm each iteration, up to a maximum radius of 4 mm. Virtual cells were added at a uniform areal density as the boundary was expanded. The marginal growth tree was generated with the following parameters: total $N = 10{,}000$ cells, DOI = 1,000 μm, VCD = 150 μm, radius growth rate = 12.5 μm per iteration, step size = 50 μm and radius of terminal vessels = 25 μm.

Gallium evacuation rates during ESCAPE in large vascular trees

Space colonization vascular trees were fabricated as described in the 'General ESCAPE process' section. In large vascular tree designs, during the evacuation of gallium with the ESCAPE process, liquid gallium flowing out from all of the terminal branches is collected through one central root vessel, for example, in the designs in Fig. 3d. To investigate whether the gallium evacuation during the ESCAPE process was limited by the flow rates through this central vessel, the evacuation of this tree was compared when 20 mM NaOH and 100 mM NaOH solutions were used (Extended Data Fig. 8c,d). When exposed to high concentrations of NaOH, the surface oxide at all branches is removed, causing all of the terminal branches to evacuate at once, as opposed to a more directional evacuation at lower concentration. This experiment shows that liquid gallium evacuation is not limited by the flow rate of liquid exiting through the parent vessel but by how many terminal branches are actively pumped out simultaneously (Supplementary Video 12).

3D applications of ESCAPE—vascular networks, orthogonal networks and cardiac bundles

In 3D architectures such as the overhand knot (Fig. 2d), 3D hierarchical tree (Fig. 3f), orthogonal networks (Fig. 4b) and cardiac bundles (Fig. 4e), narrow walls were projected onto the substrate to make the

designs mouldable to generate the PDMS negative (see Extended Data Figs. 5, 9, 10 and 11). In general, the supporting walls are made to be thinner than the smallest feature of the design such that a pressure threshold can be found so that Ga can be selectively injected into the desired portions of the PDMS negative and not the thin walls. In these designs, on solidification of the Ga cast, the PDMS negative is selectively etched to release the Ga cast, as described in the 'General ESCAPE process' section. In the overhand knot and 3D hierarchical tree examples, ECs are seeded into the channels, cultured under flow and imaged as described previously.

In the orthogonal network design, the Ga cast includes the interwoven lymphatic and blood networks and an extra Ga supporting structure to register the pieces together (Extended Data Fig. 10c,d). In this device, an external PDMS structure ensures that the collagen gel is added only in the central portion of the structure featuring the two networks, that is, the supporting arc is designed to fall outside the gel region. The port connected to the lymphatic inlet and the two ports connected to extreme ends of the blood network are isolated from each other using agarose (5% w/v of ultralow-gelling-temperature agarose; #A5030, Sigma-Aldrich) as a sealant. This scheme allows us to generate completely distinct and orthogonal cavities with ESCAPE. For cell seeding, the lymphatic ECs were first lifted from culture dishes (suspension density approximately 1×10^6 cells ml^{-1}) and seeded into the dead-ended lymphatic network, as described in the 'General device seeding and culture' section. These devices were transferred to the incubator (static culture) for 4 h for the lymphatic ECs to attach to the collagen gel. Blood ECs (hMVECs) were subsequently lifted from culture dishes, brought into suspension (density approximately 1×10^6 cells ml^{-1}) and seeded into the blood network. These devices were returned to the incubator and cultured on a rocker oriented such that flow is directed along the blood network.

The cardiac bundle design incorporates two noteworthy features (Extended Data Fig. 11a,b): first, alignment tabs are used at the extreme ends of the device to register the Ga pieces corresponding to the cardiac regions and the nearby vascular conduit. Second, the tubes gradually taper at the ends down to 70 µm diameter (shown on the right), so that cardiac cells can be intentionally brought to clog at the right ends to maximally pack cardiac cells. The Ga cast was evacuated as per the general ESCAPE process; here, again, the alignment tabs fall outside the gel region. The cardiac regions of these devices were first seeded with a cell suspension containing a mixture of iPSC-CMs (90%) and CFs (10%) at a combined cell density of 2.22×10^6 cells ml^{-1}. At this cell density, the cells clog at the tapered ends and backfill to form maximal packing densities throughout the cardiac bundle region (Extended Data Fig. 11c). These cardiac-only devices were cultured in media containing high-glucose DMEM (Fisher Scientific) supplemented with 10% FBS (MilliporeSigma), 1% penicillin–streptomycin, 1% non-essential Amino Acids (Fisher Scientific), 1% GlutaMAX (Fisher Scientific), 5 µM Y-27632 (#1254; Tocris Bio-Techne) and 0.033 mg ml^{-1} aprotinin (MilliporeSigma). Aprotinin and Y-27632 were removed from culture media after 1 day and media was replaced daily. To generate devices with both cardiac bundles and EC-lined vasculature, cardiac cells were seeded first as described above. After 1 day of culture, the media was changed to EGM2-MV and the devices were placed on the rocker for at least 4 h to prepare the vascular conduits for EC seeding. mRuby-hUVECs were seeded on to the vascular conduits at a cell suspension of 1×10^6 cells ml^{-1}. The smaller size and the lower cell suspension density prevented the ECs from clogging (unlike the iPSC-CMs in the cardiac portions) and getting packed throughout the vascular conduits. These devices were returned to the rocker with EGM2-MV as the maintenance media for two further days for the ECs to form a confluent monolayer. Live imaging was performed for both sets of devices using 4× and 10× objectives on a Nikon Eclipse Ti microscope (Nikon Corporation) in an environment-controlled chamber (humidified; 37 °C with 5% CO_2). Devices were electrically stimulated using 20-V waveforms (Extended Data Fig. 11e) generated with an IonOptix C-Pace EP cell-culture stimulator (IonOptix) and delivered using platinum wires (#EP1330; Sigma-Aldrich CVS10 replacement platinum wire; MilliporeSigma) immersed in the two furthest media reservoirs. Cardiac contractions were recorded at a frame rate of 30 FPS (Supplementary Video 14). To study the effect of cardiac contractions on the flow through the vascular conduit, 5 µl of beads were added at 1:1,000 dilution (Polybead Dyed Microsphere Kit – 1 µm; #16906-1, Polysciences) to one of the vascular media reservoirs to create a small pressure head. Kymographs (position–time maps) were generated along specific paths in the acquired videos (30 FPS frame rate) with ImageJ to map the flow of tracer beads (Extended Data Fig. 11g and Fig. 4h).

Data availability

The main data supporting the findings in this study are available in the main text, methods and Supplementary Information. Other data generated or analysed are available from the corresponding authors on request.

Code availability

Blender/Python code used to computationally generate vascular trees, OpenSCAD code to generate CAD designs and MATLAB code to analyse images are available from the corresponding authors on request.

40. Doyle, A. D. Generation of 3D collagen gels with controlled diverse architectures. *Curr. Protoc. Cell Biol.* **72**, 10–20 (2016).
41. Song, H.-H. et al. Transient support from fibroblasts is sufficient to drive functional vascularization in engineered tissues. *Adv. Funct. Mater.* **30**, 2003777 (2020).
42. Lian, X. et al. Directed cardiomyocyte differentiation from human pluripotent stem cells by modulating Wnt/β-catenin signaling under fully defined conditions. *Nat. Protoc.* **8**, 162–175 (2013).
43. Zhang, K. et al. Plakophilin-2 truncating variants impair cardiac contractility by disrupting sarcomere stability and organization. *Sci. Adv.* **7**, eabh3995 (2021).
44. Bilodeau, R. A., Zemlyanov, D. Y. & Kramer, R. K. Liquid metal switches for environmentally responsive electronics. *Adv. Mater. Interfaces* **4**, 1600913 (2017).
45. Kleiman, M., Ryu, K. A. & Esser-Kahn, A. P. Determination of factors influencing the wet etching of polydimethylsiloxane using tetra-*n*-butylammonium fluoride. *Macromol. Chem. Phys.* **217**, 284–291 (2015).

Acknowledgements S.S. thanks H. Shea and R. C. Hayward for their comments and discussions. We gratefully acknowledge support from the NIH National Institute of Biomedical Imaging and Bioengineering (NIH-EB00262, NIH-EB033821), National Science Foundation Engineering Research Center on Cellular Metamaterials (EEC-1647837), National Science Foundation Science and Technology Center for Engineering Mechanobiology (CMMI-1548571), Allen Distinguished Investigator programme, U.S.-Israel Binational Science Foundation (BSF 2017239), American Heart Association Postdoctoral Fellowship (20POST35210045), NIH National Heart, Lung, and Blood Institute (F31HL156517), NIH T32 Quantitative Biology and Physiology training grant and the Portuguese Foundation for Science and Technology (FCT; doctoral grant SFRH/BD/129224/2017).

Author contributions S.S. and C.S.C. conceived and designed the research. S.S. designed the process, wrote custom code, analysed data and was involved in all aspects of the work. S.S., J.H.L. and I.M.B. performed experiments. S.S. and C.M. printed two-photon direct writing moulds under the supervision of A.E.W. S.K. advised on cell experiments. A.L. performed multiphoton microscopy optimization. J.F.M. co-supervised the work of I.M.B. S.S., J.E. and C.S.C. wrote the manuscript. All authors discussed and contributed to the manuscript.

Competing interests A patent application (U.S. application no. 18/422,963) has been filed by Boston University based on this work. C.S.C. is a founder and owns shares in Innolign Biomedical, a company that is developing engineered organ models for pharmaceutical research and development, and Satellite Biosciences, a company that is developing cell-based therapies. The other authors declare no competing interests.

Additional information
Supplementary information The online version contains supplementary material available at https://doi.org/10.1038/s41586-024-08175-5.

Correspondence and requests for materials should be addressed to Subramanian Sundaram or Christopher S. Chen.

Peer review information *Nature* thanks Michael Bartlett, Derek Rosenzweig and the other, anonymous, reviewer(s) for their contribution to the peer review of this work.

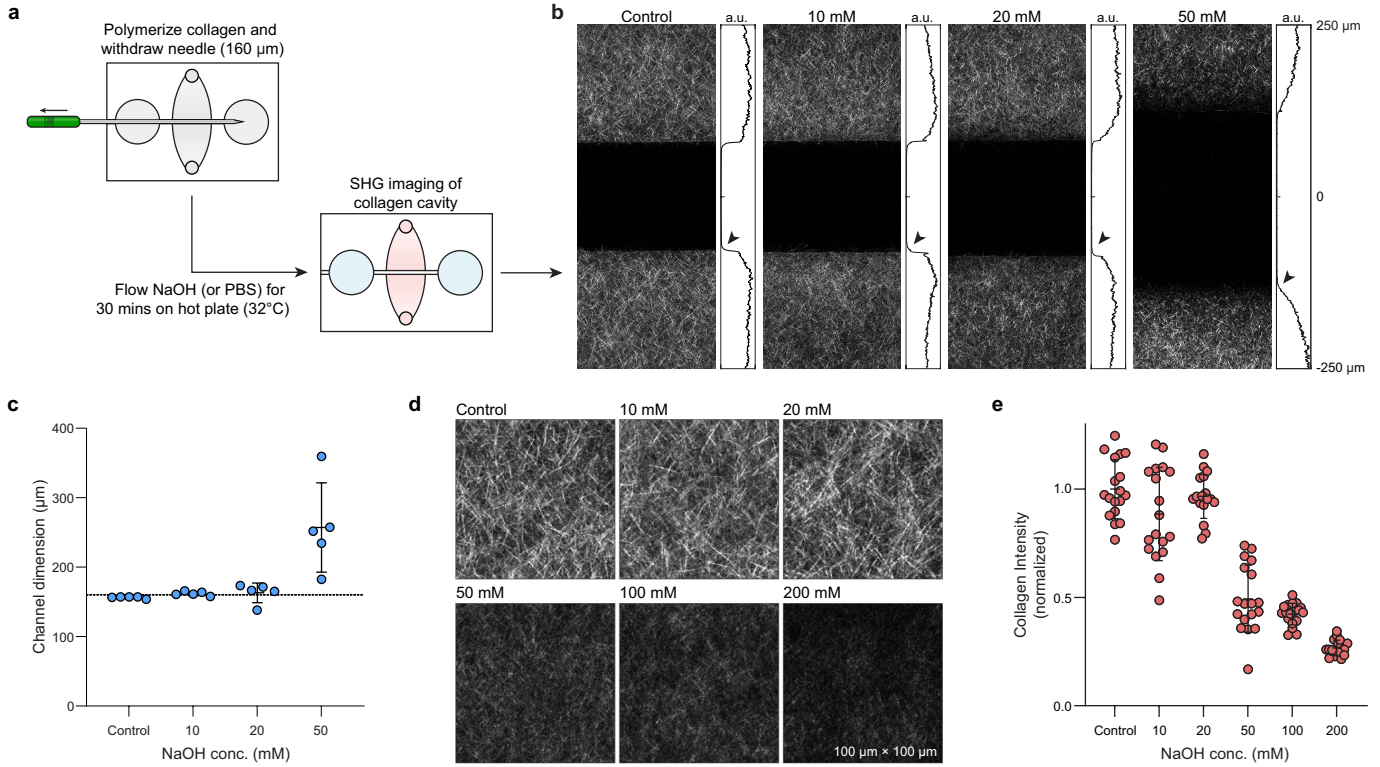

Extended Data Fig. 1 | Characterization of the dimensional stability and architecture of collagen gels on exposure to NaOH. a, To study the dimensional stability of features in collagen, we polymerized collagen gels around acupuncture needles (160 µm diameter; see Methods). After polymerizing collagen, we withdrew the needle and added different concentrations of NaOH to the reservoirs ensuring flow through the channel and placed devices on a hotplate maintained at 32 °C for 30 min. **b**, Post NaOH treatment, we imaged these collagen gels using SHG imaging. Until 20 mM NaOH treatment, the dimension of the channel closely matched the size of the acupuncture needles and the quantification of the collagen intensity showed clear boundaries (see arrows). After 30 min exposure to 50 mM NaOH, the gels lost their structural integrity, leading to broadening of the features. Gels treated with 100 mM NaOH did not show clear edges and dimensions of the channels could not be measured (not shown here). **c**, Quantification of the channel dimensions post-exposure to different concentrations of NaOH for 30 min (mean ± s.d. across five devices per concentration). **d**, Collagen architecture post 30-min exposure to NaOH as observed through SHG imaging of bulk collagen gels (regions shown are 100 µm × 100 µm). **e**, Collagen intensity changes in response to different concentration of NaOH post 30-min exposure normalized with respect to the PBS control (mean ± s.d. across 18 measurements from six devices per concentration).

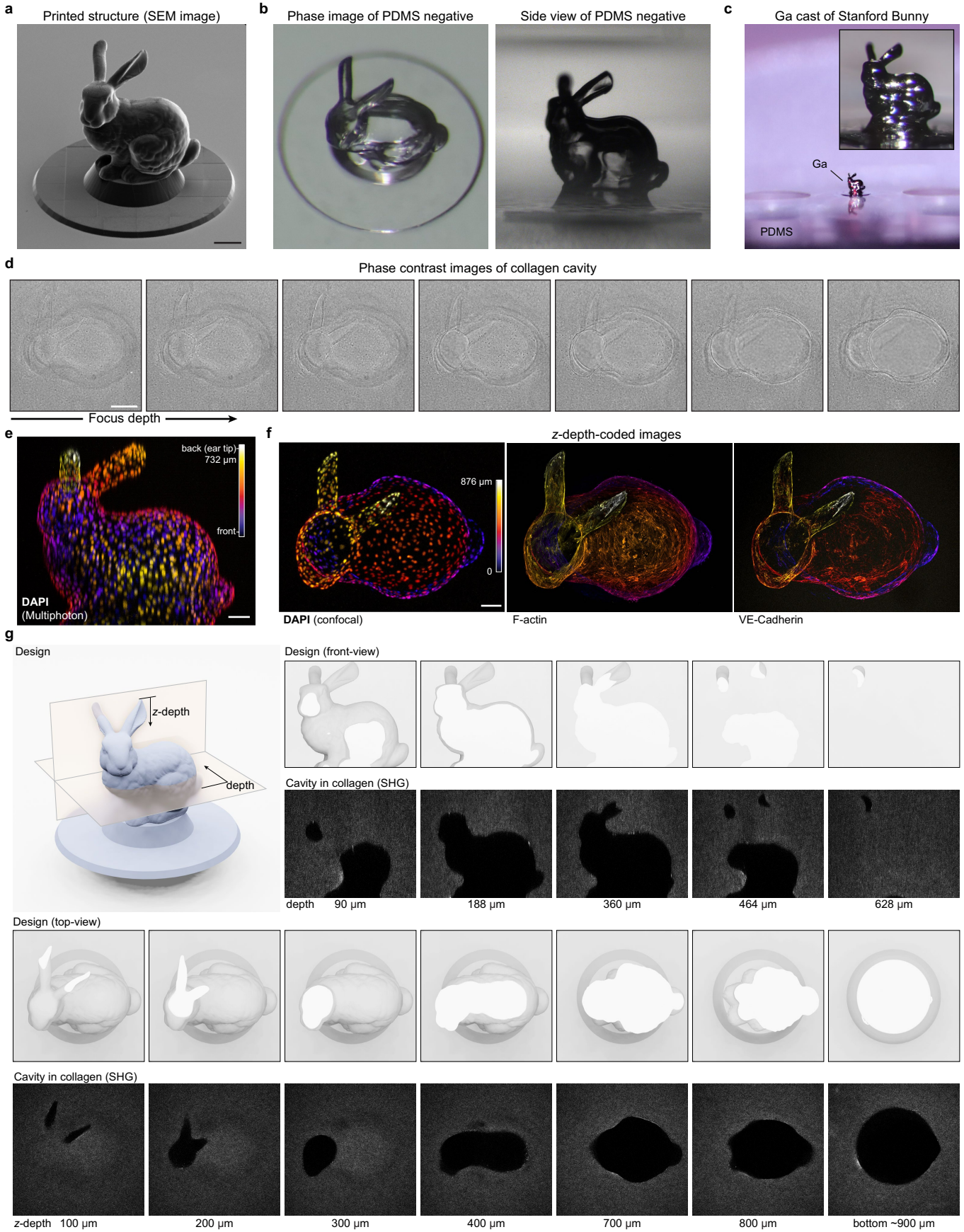

Extended Data Fig. 2 | 3D cavities in collagen. a, Printed Stanford bunny. **b**, PDMS negative. **c**, Solid Ga cast. **d**, Cavity in collagen. **e**, Depth-coded projection of cell nuclei post cell seeding. **f**, Confocal image projections of DAPI, F-actin and VE-cadherin. **g**, Comparison of 3D design (sections shown in white) and the fabricated cavity (collagen SHG signal). Scale bars, 200 µm (**a**,**d**); 100 µm (**e**,**f**).

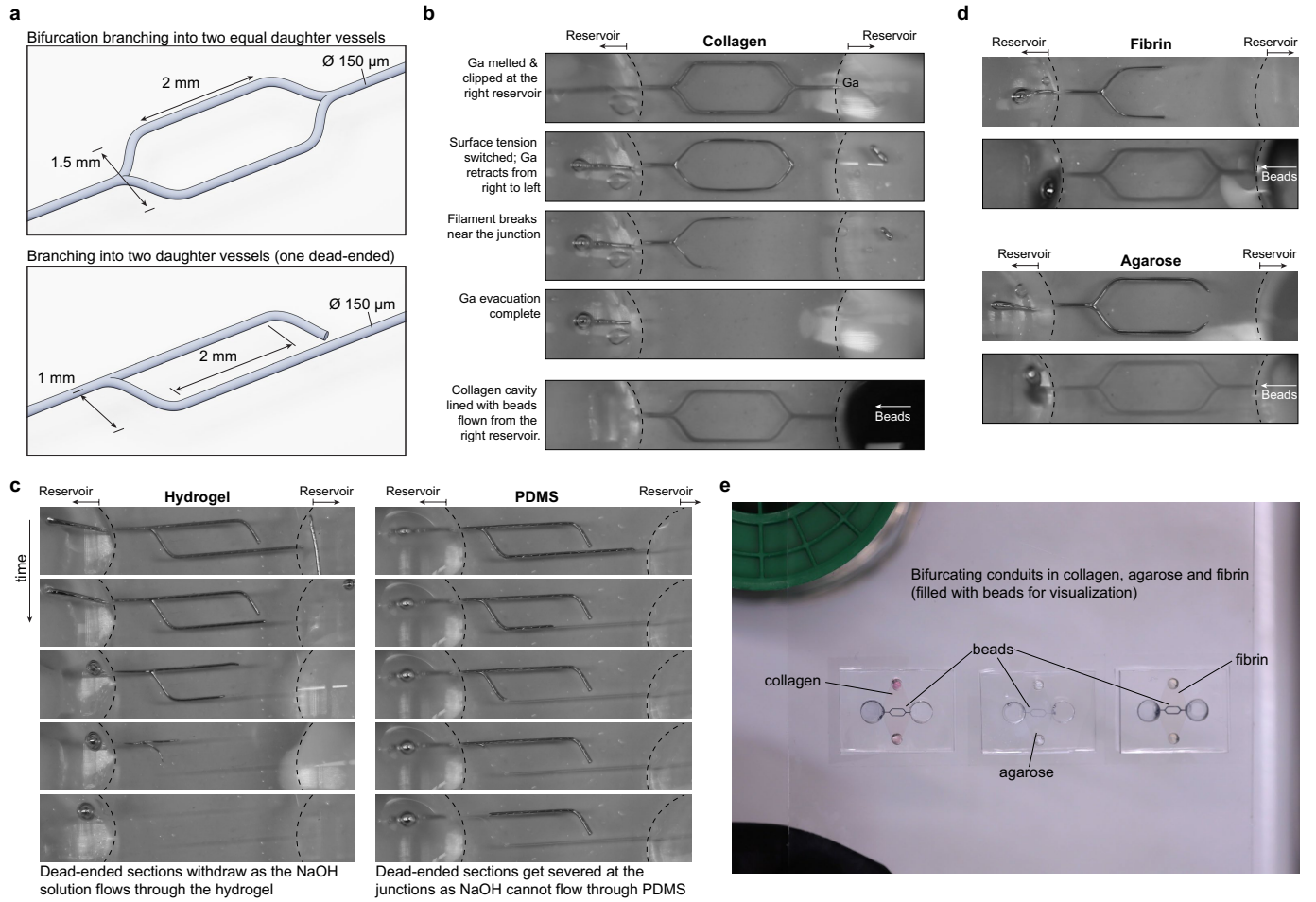

Extended Data Fig. 3 | Capillary pumping (Ga ESCAPE) in different materials. **a**, Design of bifurcations for making Ga casts. **b**, Ga can be evacuated in soft materials such as collagen. On removing the Ga cast, the empty cavity can be filled with cells or other materials; here the branching conduits are filled with coloured beads for visualization. **c**, Geometries with both flow-accessible conduits and dead ends can be retracted at once. Critically, this differs from using Ga as a sacrificial material with non-porous surrounding materials (for example, PDMS) without interstitial flow, in which dead-ended branches are severed during evacuation. **d**, Retraction process works in other soft hydrogels, such as fibrin or agarose. **e**, Photographs of devices with different materials after Ga retraction with coloured beads lining the conduits. **f**, Culturing cells in direct contact with Ga does not result in cell toxicity. **g**, Cells grow on top of Ga (probably on the native oxide layer) when cultured on dishes containing Ga droplets. Scale bars, 100 µm. Dead cells could be seen occasionally (marked by white arrowheads on the right) at the contact line between Ga and the culture dish, which—we posit—is from the increased mechanical movement of the interface at the contact line.

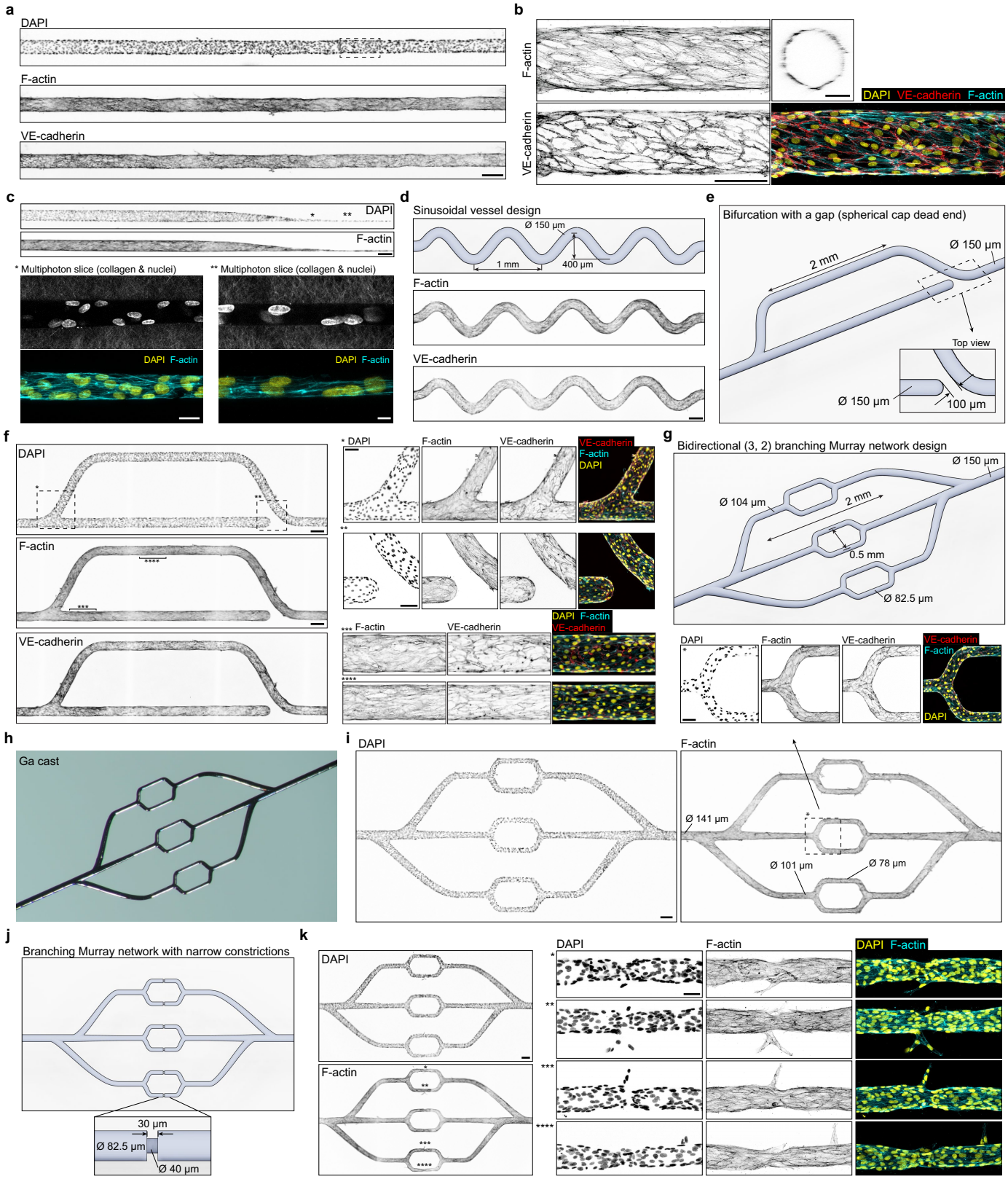

Extended Data Fig. 4 | Endothelialized vessels. a, 150-µm-diameter cylindrical vessel seeded with ECs. Scale bar, 200 µm. **b**, Close-up of the vessel showing F-actin and VE-cadherin (scale bar, 100 µm) and the cross-section (scale bar, 50 µm). **c**, Tapered vessel with calibre decreasing from 150 µm to 20 µm. Scale bar, 200 µm. Close-up multiphoton images show collagen and the cell nuclei in a single plane. Corresponding confocal maximum projections show that cells line the vessels uniformly until the cavity is comparable in size to the cell nuclei (scale bars: left, 25 µm; right, 10 µm). **d**, Sinusoidal vessel design and fabricated device. Scale bar, 200 µm. **e**, Bifurcating vessel with one dead-ended branch and maximum projections of the fabricated device (**f**; scale bar, 200 µm). The close-up images show the perfused and dead-ended sections. Scale bars, 100 µm. **g**, Two-level branching Murray design. Ga cast (**h**) and immunofluorescence images (**i**). Scale bars, 200 µm (tile scan); 100 µm (close-up image). **j**, The two-level branching design with narrow constrictions in the smallest branches (**j**) and the fabricated device (**k**; scale bar, 200 µm). Close-up images show four constricted sections (scale bar, 50 µm).

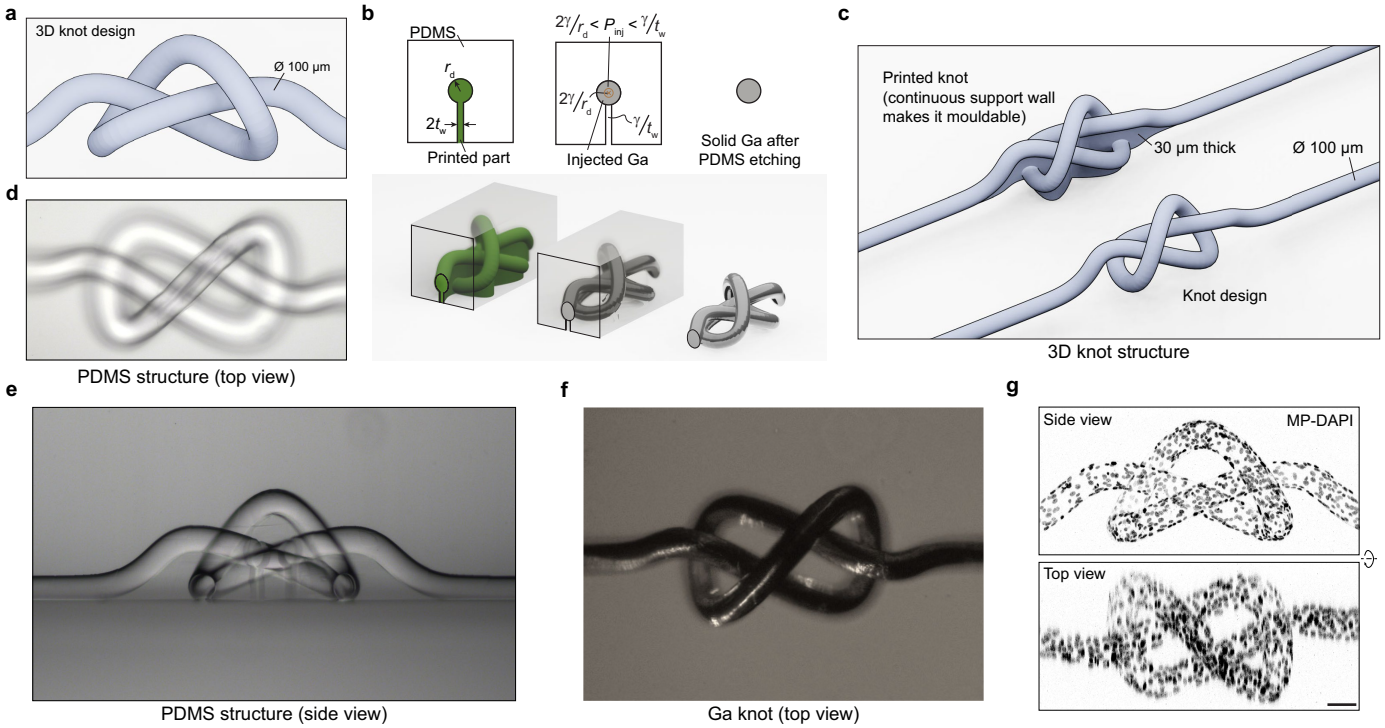

Extended Data Fig. 5 | Self-intersecting structures. a, 3D knot design. **b**, By introducing a narrow continuous wall under the part, self-intersecting structures such as the knot can be moulded. The thickness of the wall is made to be much smaller than the feature. After demoulding the negative structure, the high surface tension of the liquid is used in controlling where Ga flows, that is, the injection pressure is greater than the value required to inject Ga into the knot itself but not high enough for entering the gap left by the narrow wall. **c**, The modified design of the knot used for printing and the resulting shape of the Ga cast. **d**, PDMS negative copy of the printed structure (side view in **e**). **f**, Photo of the moulded Ga knot. **g**, Side and top views of the cell nuclei. Scale bar, 100 µm. **h**, Immunofluorescence images of the EC-lined knot labelling F-actin and VE-cadherin. Scale bar, 100 µm.

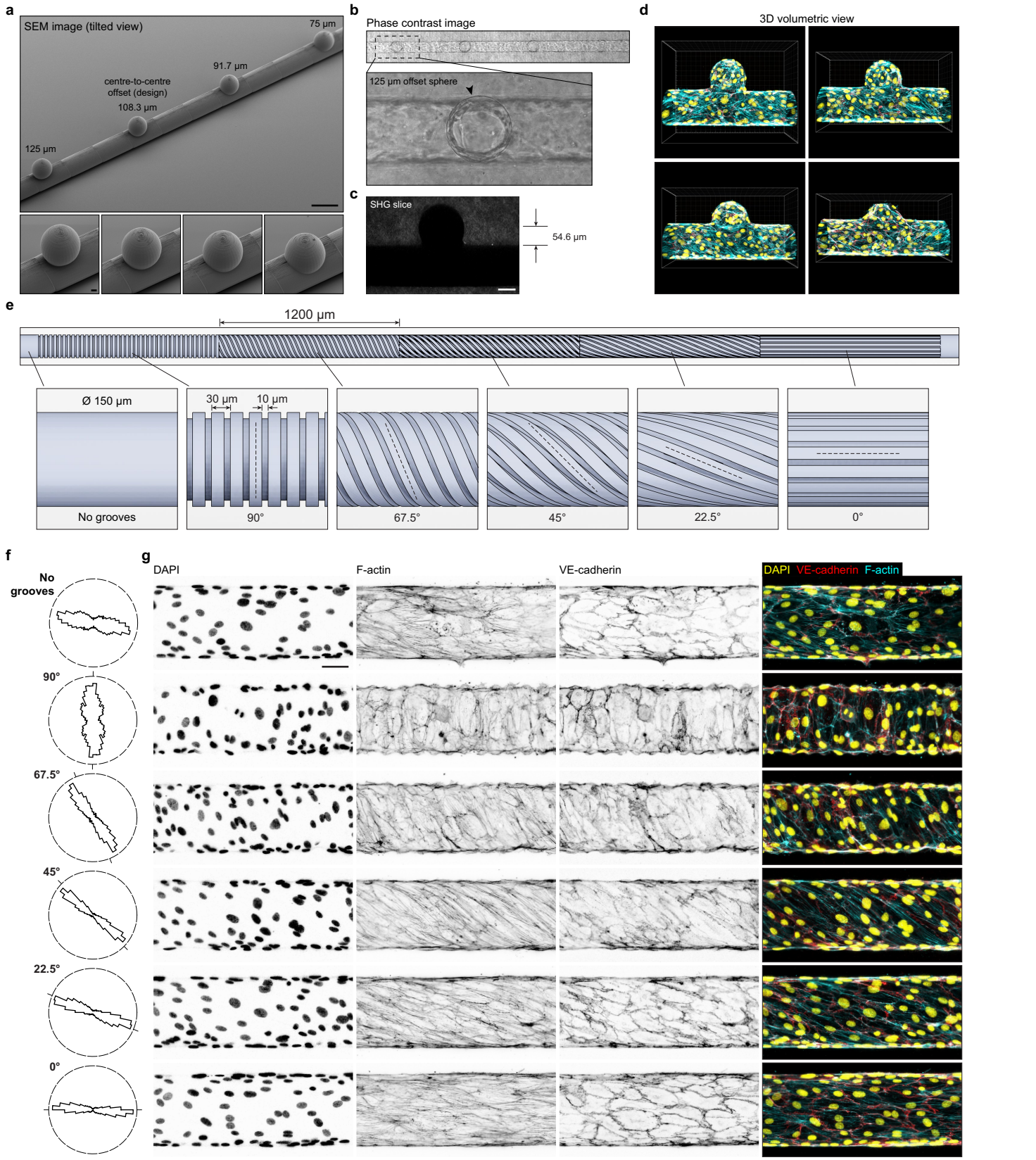

Extended Data Fig. 6 | Fine control of vascular structures—vascular malformations and microgrooves to control cell alignment. a, Tilted-angle SEM images of the printed vascular malformation design. Scale bar, 200 µm. Close-up images show spherical blebs with different offsets. Scale bar, 20 µm. **b**, Phase-contrast image of the collagen device seen from top of the blebs. The fabrication process yields high-resolution smooth spherical blebs (shown by the arrowhead). **c**, SHG slice of collagen (averaged) through one bleb structure before cell seeding. Scale bar, 50 µm. **d**, 3D volumetric views of the different spherical blebs. **e**, Design of a cylindrical vessel with no orientation cues and five regions to align cells progressively from 90° to 0° (along the length of the vessel). **f**, Orientation histograms of the cells (F-actin) at different regions of the vessel. **g**, Half vessel maximum projections of DAPI, F-actin and VE-cadherin at different vessel regions. Scale bar, 50 µm.

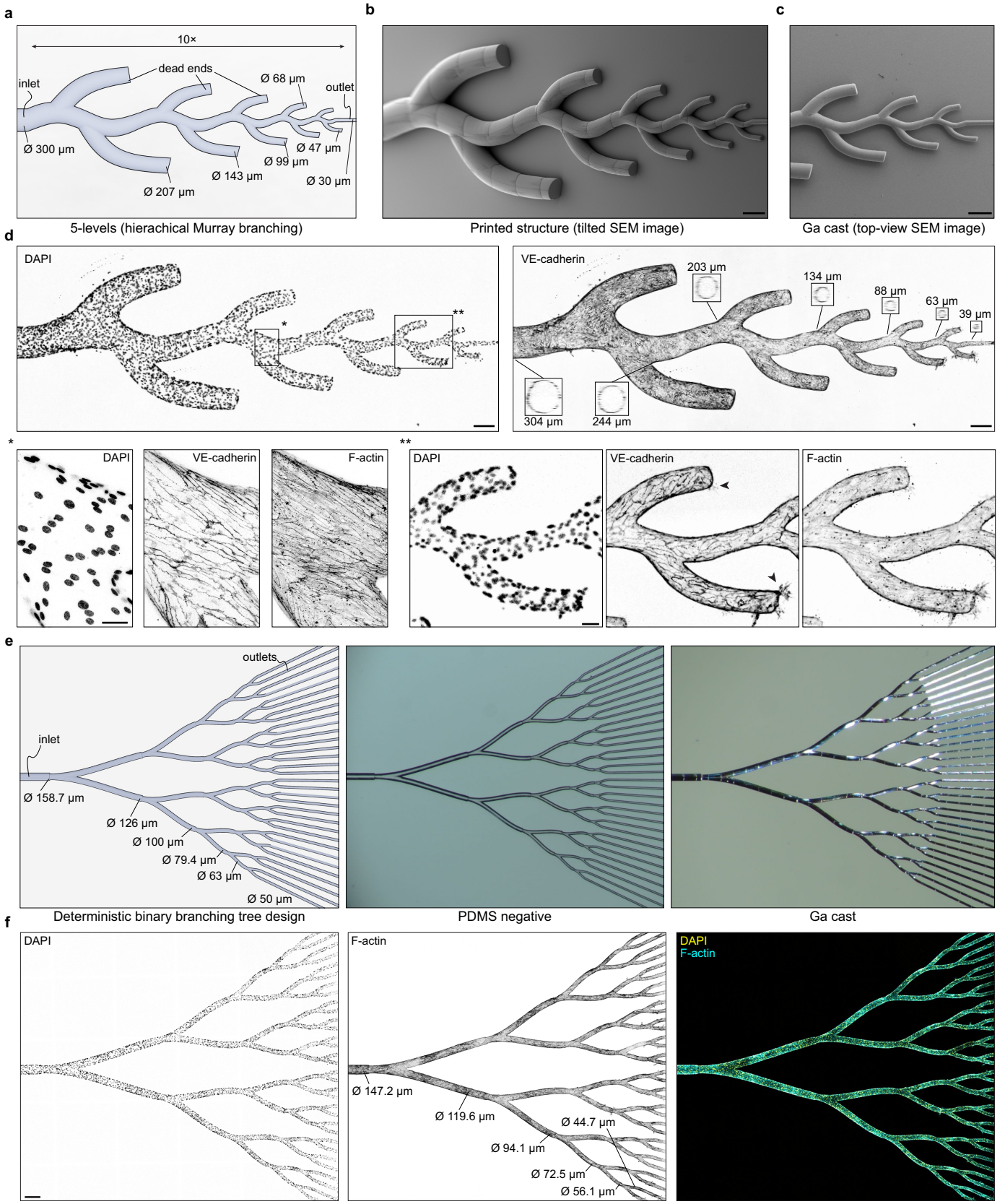

Extended Data Fig. 7 | Hierarchical branching trees with both perfused and dead-ended sections. a, Branching vessel architecture with a tenfold reduction in vessel calibre. The vessels are dimensioned according to Murray's law (with exponent 2.96) at each branching hierarchy. **b**, Tilted-angle SEM images of the printed structure. Scale bar, 200 µm. **c**, SEM image of the smallest branches of the Ga cast. **d**, Tile scan of the device showing the cell nuclei and VE-cadherin. The insets show vessel cross-sections at different regions of the device. Scale bar, 200 µm. The close-up images (bottom) show a branch point and cells sprouting from the dead ends at approximately 60-µm-sized vessels. Scale bars, 50 µm. **e**, Design of a deterministic tree with symmetric bifurcations with each vessel (perfusable). **f**, Maximum projection of tile scans of the deterministic binary tree. Scale bar, 250 µm.

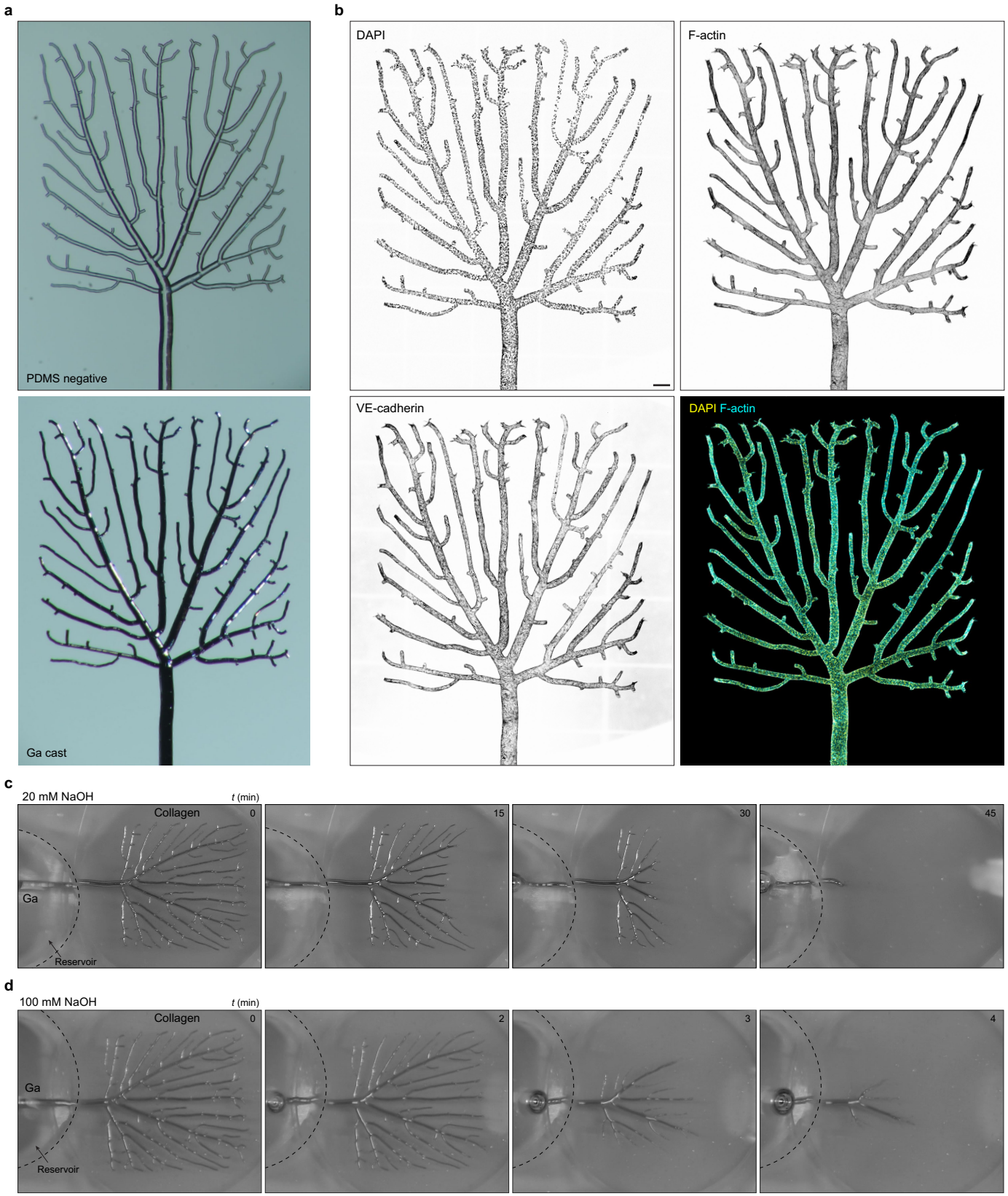

Extended Data Fig. 8 | Rectangular tree. a, PDMS negative of the 4 × 4-mm^2 tree. **b**, Tile scan of the vascular tree showing the cell nuclei and F-actin. Scale bar, 250 µm. **c**, Time-course images of the Ga retraction process with 20 mM NaOH (see Supplementary Video 12). **d**, When high concentrations of NaOH are used, the retraction process is expedited, showing that the retraction rate is determined by how the surface oxide is removed (spatially) and not limited by the evacuation rate of liquid Ga through the central root.

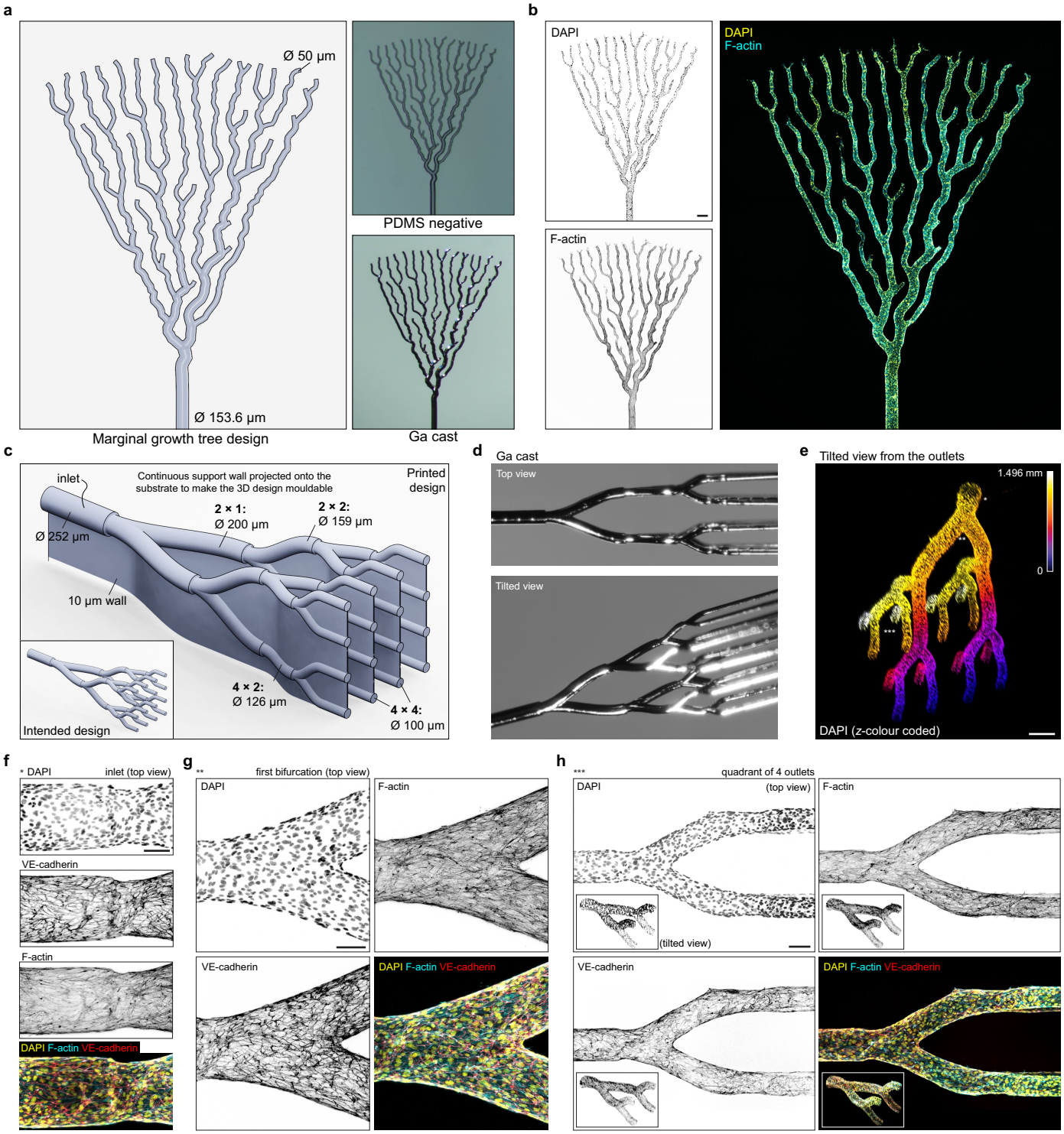

Extended Data Fig. 9 | Marginal growth and hierarchical 3D vascular trees. **a**, Design generated through marginal growth (in which the boundary is grown iteratively; see Methods), the corresponding PDMS negative and the Ga cast. **b**, Tile scan of the marginal growth tree showing F-actin and DAPI. Scale bar, 250 µm. **c**, Hierarchical 3D vascular tree design branching from one inlet to 16 outlets, with the branches sized per Murray's law. The projected thin support wall (10 µm thick) makes the printed 3D structure mouldable, that is, PDMS can be polymerized around this structure and removed. Subsequently, when liquid Ga is injected into the mould, it preferentially fills the branching vascular structure (all features ≫10 µm) but not the narrow wall yielding a cast of the intended design. **d**, Photographs of the gallium cast as viewed from the top and when tilted. **e**, Tilted (volumetric) view of the cell nuclei of the endothelial monolayer through SHG imaging as viewed from the array of outlets; colour denotes the vertical position. Scale bar, 300 µm. Maximum projections of the inlet (**f**), the first bifurcation (**g**) and a quadrant of outlets (**h**) showing DAPI, VE-cadherin and F-actin. Scale bars, 100 µm. The insets in **h** show the corresponding regions in a titled volumetric view. The regions shown in **f**, **g** and **h** are marked in the full device image (**e**) as *, ** and ***, respectively.

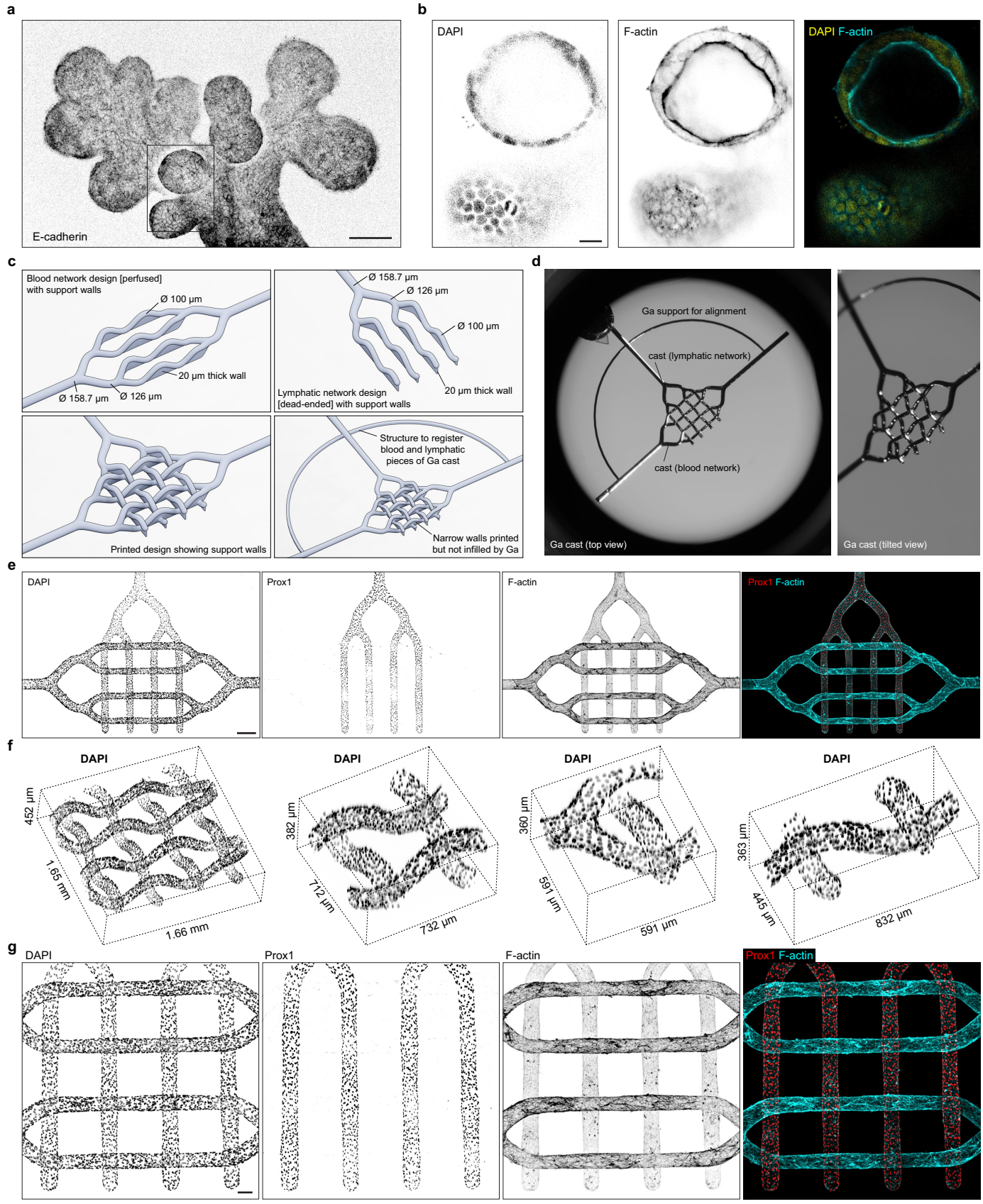

Extended Data Fig. 10 | Applications—epithelial buds and orthogonal (blood and lymphatic) networks. a, Maximum projection of the 3D epithelial bud geometry (E-cadherin). Scale bar, 100 µm. **b**, The close-up images show the cell nuclei and F-actin at a slice through a single bud. Scale bar, 20 µm. **c**, Design of the 3D, enmeshed blood and lymphatic networks and supporting structures. The enmeshed architecture requires thin support walls (20 µm thick) projected onto the substrate to make the design mouldable. The Ga pieces corresponding to the blood and lymphatic network are aligned with respect to each other through a supporting structure (outside the device/gel region). **d**, Ga cast. **e**, Maximum projections of the device. Scale bar, 300 µm. Volumetric (**f**) and close-up projections (**g**; scale bar, 100 µm) of the enmeshed parts of the device (see Fig. 4b–d).

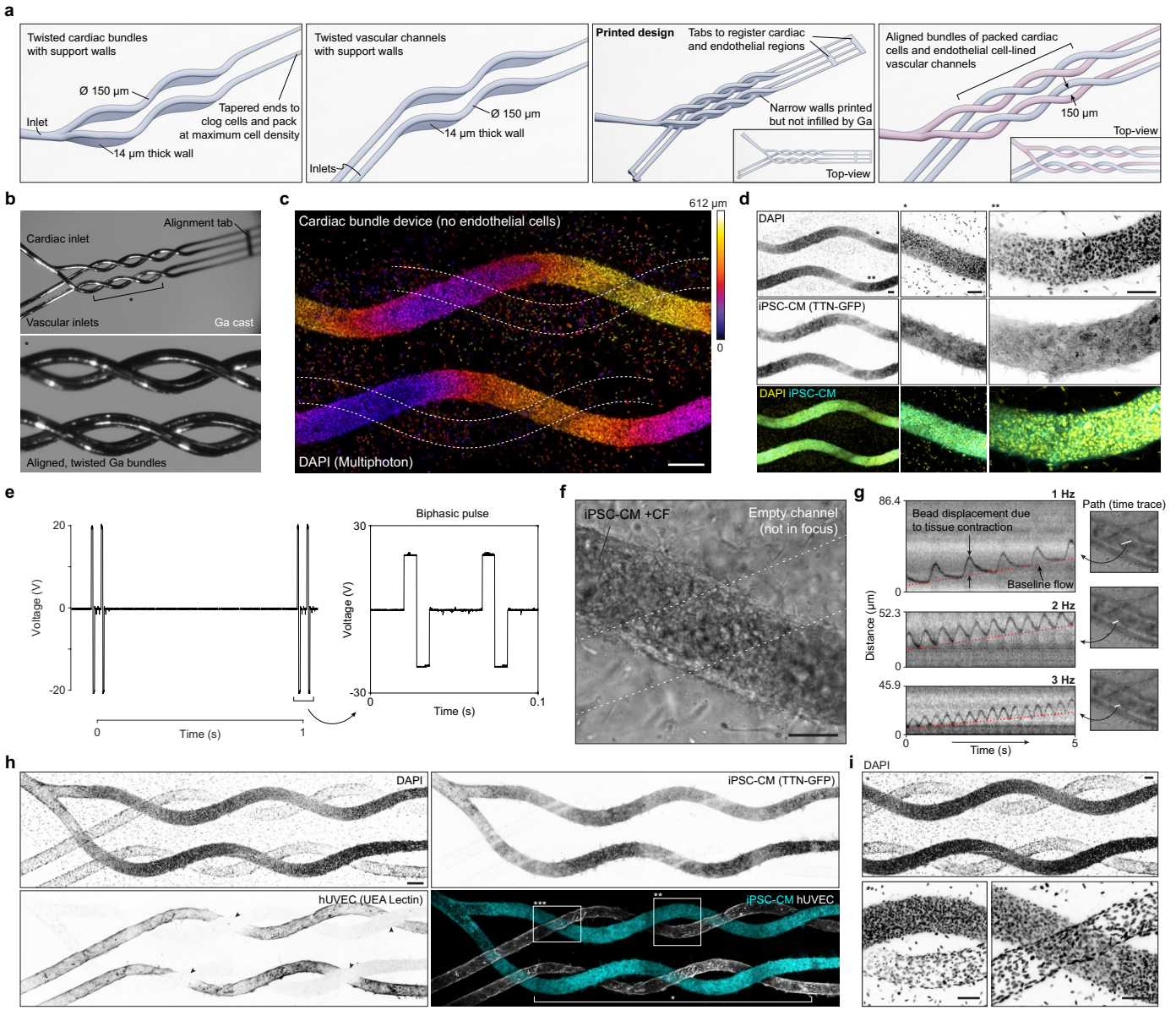

Extended Data Fig. 11 | Cardiac bundles with vasculature. a, Design consists of helical cardiac bundles maximally packed with iPSC-CMs (90%) and CFs (10%) twisted along with aligned vascular channels separated by 150 µm. Thin supporting walls projected onto the substrate (14 µm) are used to make the design mouldable. Tabs at the right end hold the cardiac and vascular portions of the Ga cast together at the ends of the cast. **b**, Ga casts of the twisted cardiac and vascular regions. **c**, To study the effectiveness of maximally packing cells in the cardiac portions, devices were filled with a mixture of iPSC-CMs (90%) and CFs (10%) in the cardiac portions alone and the vascular regions were left empty. Depth-coded projection of the cell nuclei. Scale bar, 200 µm. **d**, iPSC-CMs are confined to bundles and the cells in the bulk are CFs, as seen in the maximum projection images. Scale bars, 100 µm. **e**, Voltage waveforms used for 1-Hz electrical stimulation and a close-up of the biphasic pulse. **f**, Phase image of the device region showing the cardiac bundle and the vascular channel with beads (not in focus). Scale bar, 100 µm. **g**, On the addition of tracer beads into the vascular conduit, the displacement of particles can be tracked along specific paths in the form of kymographs (see Supplementary Video 15). The beads appear as black spots forming traces that show the baseline flow rate from the pressure head and the impact of cardiac contraction at different stimulation frequencies. **h**, Maximum projections of the devices containing both cardiac cells (in the cardiac portions) and a confluent layer of ECs in the vascular conduits. Scale bar, 200 µm. **i**, Close-up images showing the cell nuclei of regions marked in **h** and corresponding to Fig. 4g. Scale bars, 100 µm.